HYDRIDE PRODUCTION IN ZIRCALOY-4 AS A FUNCTION OF TIME AND TEMPERATURE

A Thesis

by

ADAM JOSEPH PARKISON

Submitted to the Office of Graduate Studies of
Texas A&M University
in partial fulfillment of the requirements for the degree of

MASTER OF SCIENCE

May 2008

Major Subject: Nuclear Engineering

HYDRIDE PRODUCTION IN ZIRCALOY-4 AS A FUNCTION OF TIME AND TEMPERATURE

A Thesis

by

ADAM JOSEPH PARKISON

Submitted to the Office of Graduate Studies of
Texas A&M University
in partial fulfillment of the requirements for the degree of

MASTER OF SCIENCE

Approved by:

Chair of Committee,	Sean McDeavitt
Committee Members,	Lin Shao
	Haiyan Wang
Head of Department,	Raymond Juzaitis

May 2008

Major Subject: Nuclear Engineering

ABSTRACT

Hydride Production in Zircaloy-4 as a Function of Time and Temperature. (May 2008)

Adam Joseph Parkison, B.S., Purdue University

Chair of Advisory Committee: Dr. Sean M. McDeavitt

The experiments performed for this thesis were designed to define the primary process variables of time, temperature, and atmosphere for an engineering system that will produce metal powder from recycled nuclear fuel cladding. The proposed system will hydride and mill Zircaloy cladding tubes to produce fine hydride powder and then dehydride the powder to produce metal; this thesis is focused on the hydride formation reaction. These experiments were performed by hydriding nuclear grade Zircaloy-4 tubes under flowing argon-5% hydrogen for various times and temperatures. The result of these experiments is a correlation which relates the rate of zirconium hydride formation to the process temperature. This correlation may now be used to design a method to efficiently produce zirconium hydride powder.

It was observed that it is much more effective to hydride the Zircaloy-4 tubes at temperatures below the α-β-δ eutectoid temperature of 540°C. These samples tended to readily disassemble during the hydride formation reaction and were easily ground to powder. Hydrogen pickup was faster above this temperature but the samples were generally tougher and it was difficult to pulverize them into powder.

DEDICATION

This thesis is dedicated to my parents, Scott and Melanie Parkison, as well as my brothers, Brian and Alex Parkison.

ACKNOWLEDGEMENTS

I would like to specially thank my committee chair Dr. Sean M. McDeavitt as well as my committee members Dr. Lin Shao and Dr. Haiyan Wang for all the help and encouragement they have given me. I would also like to thank the faculty of Texas A&M University for providing me with a great education, and for always being available whenever I needed assistance. Additional thanks go to my friends and colleagues, Aaron Totemeier, Luis Ortega, and Matt Solmos for being willing to share ideas and to give me ideas regarding this research. I would like to acknowledge the U.S. Department of Energies Nuclear Energy Research Initiative for supporting this project (NERI ID NO. DE-FC07-05ID14656). Finally, I would like to thank my family for all of their support and encouragement.

NOMENCLATURE

BCC	Body Centered Cubic
FCCI	Fuel-Cladding Chemical Interaction
HCP	Hexagonal Close-Packed
RTV	Room Temperature Vulcanizing
SCFH	Standard Cubic Feet per Hour
TRU	TRansUranic
UHP	Ultra High Purity
VAC	Volts Alternating Current
XRD	X-Ray Diffraction

TABLE OF CONTENTS

Page

LIST OF FIGURES

Page

LIST OF TABLES

1. INTRODUCTION: PRODUCTION OF ZIRCONIUM HYDRIDE POWDER

If nuclear energy is to maintain its status as a clean, safe, and reliable energy source, the nuclear waste issue must be addressed in an economic and responsible manner. The research described here is part of a larger project funded by the U.S. Department of Energy's Nuclear Energy Research Initiative that is developing a method to safely store and potentially recycle transuranic (TRU) isotopes from spent nuclear fuel. This will be accomplished by encapsulating the TRU oxides in a Zircaloy matrix cermet via powder metallurgy. [1] Therefore, the recovery of Zircaloy metal powder from spent fuel cladding is a required operation for the success of this concept.

Experiments were performed to define the fundamental mechanism and process variables of hydride formation in Zircaloy-4 in order to provide a basis for an engineering system that will ultimately produce metal powder from recycled nuclear cladding. The proposed Zircaloy recycle process will hydride and mill Zircaloy cladding tubes to produce fine hydride powder and then dehydride the powder to produce metal; the research described here is exclusively focused on understanding the hydride formation reaction. To this end, hydriding experiments were performed using nuclear grade Zircaloy-4 tubes exposed to flowing argon-5% hydrogen for various times and temperatures. Zircaloys are nominally ~98 wt. % zirconium and the composition of Zircaloy 4 cladding is shown in Table 1. [2]

This thesis follows the style of Journal of Nuclear Materials.

Table 1: Composition of Zircaloy-4.

Element	Wt % in Zircaloy-4
Sn	1.2-1.7
Fe	0.18-0.24
Cr	0.07-0.13
O	0.12
Zr	Balance

The recycle of zirconium from spent nuclear fuel cladding is desirable, in part, because the cladding material already contains "nuclear grade" zirconium, which has a very low hafnium content. As a lesser point of interest, the Zircaloy cladding becomes radioactive in service due to neutron activation and ion implantation of radioactive isotopes from the fission process. The Zircaloy becomes further degraded and contaminated via fuel-cladding chemical interactions (FCCI). As a result, it is not clear that spent Zircaloy can be discarded as low level waste, so the partial recycle of the Zircaloy "waste" into a TRU storage form may reduce the ultimate volume of high level waste attributable to reprocessing.

As stated above, the research described here focuses on quantifying the process variables for the transformation of Zircaloy cladding hulls into a zirconium hydride powder. One of the advantageous phenomena inherent in the transformation of Zircaloy cladding into zirconium hydride is that the density changes from ~6.5 g/cm^3 (ρ_{Zr} = 6.49 g/cm^3 [3]) to ~5.6 g/cm^3. [4] This difference in density coupled with the brittle nature of

zirconium hydride results in an extremely brittle zirconium hydride product which can then be easily ground into a fine powder.

The hydride formation data from this research was quantified as the metal-to-hydride conversion percent (P_H) in Zircaloy-4 tubes as a function of time and temperature. These data were used to develop an understanding of how the hydride process effects embrittlement of the cladding. A correlation for P_H as a function of time and temperature is developed in Section 5.2 based on a parabolic equation for the a α-Zr phase and a linear equation for the β-Zr phase as seen in Equations 1 and 2.

$$\begin{aligned} &\text{For } 440^{o}\text{C} < T < 540^{o}C \\ &P_H = At^m \\ &A = 0.028T - 6.39 \\ &m = 1.74 \pm 0.05 \end{aligned} \qquad [1]$$

$$\begin{aligned} &\text{For } 540^{o}\text{C} < T < 640^{o}C \\ &P_H = At \\ &A = 0.085T - 20.5 \end{aligned} \qquad [2]$$

"P_H" is degree of reaction completion in % hydride
"t" is time in hours
"T" is temperature in Celsius

Where *A* and *m* are constants which were found experimentally. The rate of hydride formation with respect to temperature can then be used to engineer a pathway along the binary Zr-H phase diagram, Figure 1

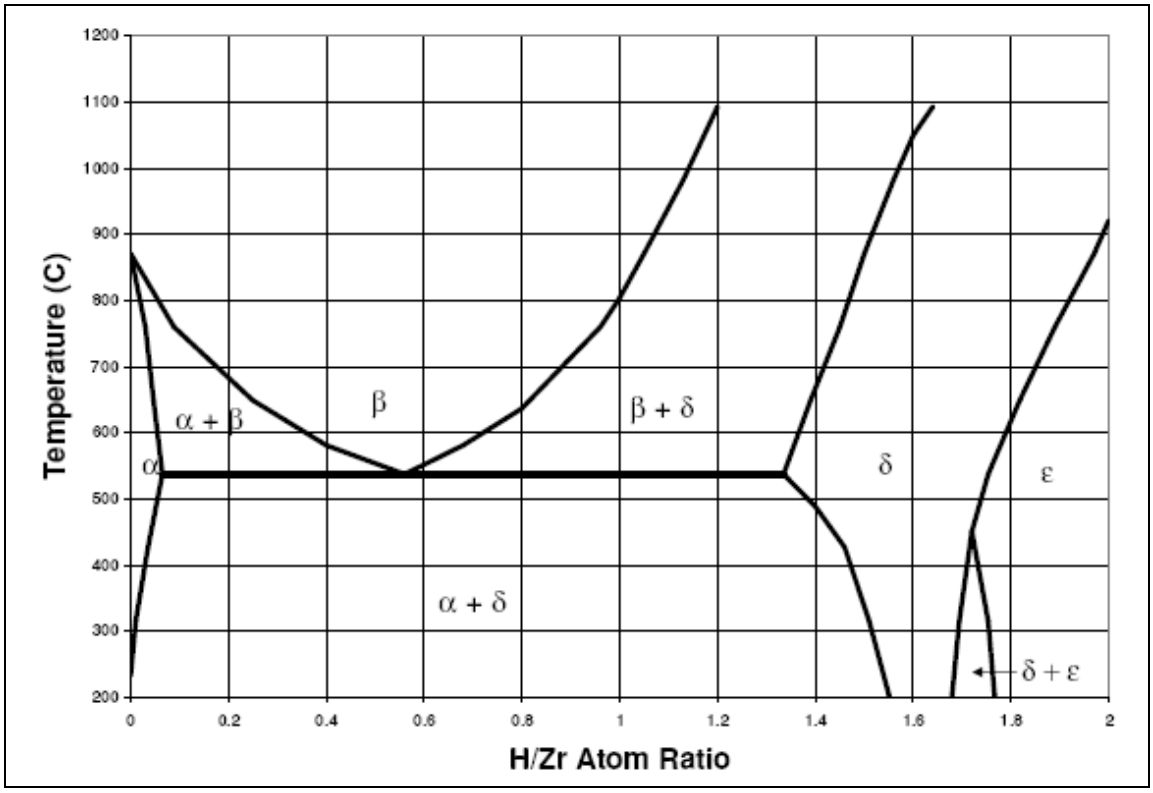

Figure 1. Hydrogen-zirconium phase diagram.

2. PREVIOUS WORK

2.1 Zirconium Processing

Industrial processes designed to produce and refine pure zirconium have been developed and implemented with varying degrees of success. These methods include, but are not limited to, sodium reduction of $ZrCl_4$, potassium reduction of ZrO_2, electrolysis of the fused salt K_2ZrF_6, the Kroll process, and the hydride/dehydride process. [5] The two reduction methods are known to both have purity issues, especially with respect to contaminating gasses such as nitrogen and oxygen. As with any electrolysis process, the fused salt method is limited for industrial use because it is expensive due to its high energy demand, and is a batch process technique. [6]

The Kroll process is by far the leading process for the production of zirconium. This process transforms zirconium ore to zirconium ingots by way of several chemical steps. The zirconium ore is processed prior to being reacted with chlorine gas to form $ZrCl_4$ along with other volatile chlorine compounds. The product is distilled and separated to generate a pure $ZrCl_4$ vapor stream. This gas is then passed over molten magnesium, resulting in the formation of $MgCl_2$ liquid and Zr sponge by the following reaction.

$$2Mg(l) + ZrCl_4(g) \rightarrow 2MgCl_2(l) + Zr(s) \qquad [3]$$

The magnesium and chlorine can later be recovered and recycled in the process. This process is useful in producing zirconium sponge as well as zirconium ingots, but is limited in its ability to produce zirconium powder. [7]

The hydride/dehydride process is known to produce a high purity zirconium powder, with a purity which is very similar to the initial purity of the zirconium to be transformed. This process is considered superior to all other methods with respect to the purity of the resulting zirconium powder. [6] Patent number 4,470,847 describes this process in detail. [8]

The hydride/dehydride process for zirconium powder production is based upon the concept that zirconium swells dramatically do to density changes as hydrogen is added to the material. It has been reported that this volume change is on the order of 8.2% to 15.4%. [7] This volume change combined with the brittle nature of zirconium hydride allows the resulting zirconium hydride to be ground to a fine powder. The zirconium hydride powder may then be dehydrided at temperatures above 800°C at low pressures, resulting in a fine zirconium powder. [6]

It is widely reported that the maximum hydrogen pickup occurs at temperatures near 300°C for all pressures. However, for the production of zirconium powder, the general practice is for the reaction to take place at 800°C. [6] This high temperature allows for rapid hydrogen absorption which is ideal for thick pieces of zirconium. The high temperature is required because the zirconium hydride reaction is a diffusion controlled process. Diffusion is known to be a temperature dependant phenomenon with a parabolic relation with respect to time. Therefore, the higher the temperature, the faster the hydride reaction will progress through the bulk of the material. [7] It is also known that the rate of the hydride reaction is proportional to the surface area of the material. A result of this is that the rate of the hydride reaction within bulk material is

dramatically lower than for a metal sponge or powder. [9] Regardless of the geometry, it has been found that the rate of hydrogen pickup within zirconium is proportional to the square root of the pressure. Given this dependence it is evident that slight differences in pressure are more important at lower pressures, while at higher pressures, variations in pressure will have less of an impact. [7]

It has been reported that it is necessary to have a concentration of 50 atom percent hydrogen within the zirconium matrix in order for the zirconium hydride sample to easily grind to powder. This is the recommended hydrogen concentration for zirconium hydride materials which have been produced at high temperatures such as 800°C. This corresponds to a regime where hydrogen is diffusing through the body-centered cubic (BCC) β-Zr phase, which is known to be a more stable phase than the hexagonal close-packed (HCP) α-Zr phase. [6]

Further, the reaction rate of hydrogen with zirconium is known to be dependent on surface effects. These surface effects may include films left from the processing of the material, as well as the oxide surface layer. It is therefore essential to thoroughly clean specimens which are to be reacted. It has been found that the oxide surface layer may be dissolved into the bulk Zr lattice by preheating it at 1050°C. This surface oxide layer plays an important role at low temperature. In fact, the hydride rate has been seen to be up to 7700 times higher for these heat treated materials than for the materials which contain an oxide surface layer at 150°C. The heat treatment of zirconium has been seen to have an effect on the hydride reaction at heat treatment temperatures as low as 500°C. [7]

When hydrogen is reacted with zirconium, it occupies the tetrahedral positions of the HCP alpha and BCC beta phases. However, when elements such as oxygen or nitrogen react with zirconium, they occupy the octahedral positions of the HCP alpha and BCC beta phases. These oxygen or nitrogen atoms cause local distortions in the metal lattice making it impossible for hydrogen to locate itself in the nearby tetrahedral positions. This effect has been seen to cause a strong dependence of oxygen or nitrogen content within the metal on the hydride reaction rate. It is therefore of the utmost importance to have a clean, nitrogen and oxygen free system in order for the hydride reaction to progress quickly. Specifically, nitrogen is the element of most interest when considering this effect, and has the largest impact on decreases in the reaction rate of hydrogen and zirconium. [7]

2.2 Previous Hydride Process Development Experiments

This thesis is a continuation of work performed by Dustin Kraemer, the results of which can be seen in reference 3. The work performed by Kraemer focused on the design and construction of an experimental system which can be used to produce a zirconium hydride powder, using the hydride process. The original system which was designed and built by Kraemer was the foundation for the experimental setup used in this thesis. Kraemer performed 14 proof of concept experiments which gave a basic understanding of the behavior of the system for various temperatures, pressures, and hydride times. It was observed that zirconium hydride produced in the alpha phase was more brittle than zirconium hydride produced in the beta phase. It was also observed that the hydride reaction proceeded more rapidly at higher pressures than for lower

pressures. These results indicated that zirconium hydride could be produced and then turned to powder by grinding with a mortar and pestle.

3. EXPERIMENTAL DESIGN AND PROCEDURE

The hydride formation experiments were performed on nuclear grade Zircaloy-4 tubes by exposing them to flowing argon - 5% hydrogen process gas, with time and temperature as process variables. The experimental setup is an improved version of the system described by Kraemer [3] and it consists of a controlled atmosphere reaction vessel containing a small sample of Zircaloy-4. The vessel is a sealed alumina tube with flowing Ar-H_2 gas and is inserted into a tube furnace. The system is loaded and unloaded inside of an inert argon atmosphere glovebox to minimize the contamination of the hydride product from contaminants in the air, most notably nitrogen, oxygen, and water. Following the scoping project reported by Kraemer, which included 14 proof of principle experiments, 87 experiments were carried out to fully define the hydride formation process. Appendix A shows a complete summary of these experiments, and the results are described in Section 4.

3.1 Experimental Design

3.1.1 Process Gas Flow

Figure 2 shows the schematic of the gas delivery system. The process gas source comes from two separate gas cylinders. One cylinder contains ultra high purity (UHP) argon and the second cylinder contains Ar-5%H_2. The UHP argon was used during and after experiment 51. Previous to this, welder's grade argon was used, but it was found that welder's grade argon was not pure enough to get consistent results for this process

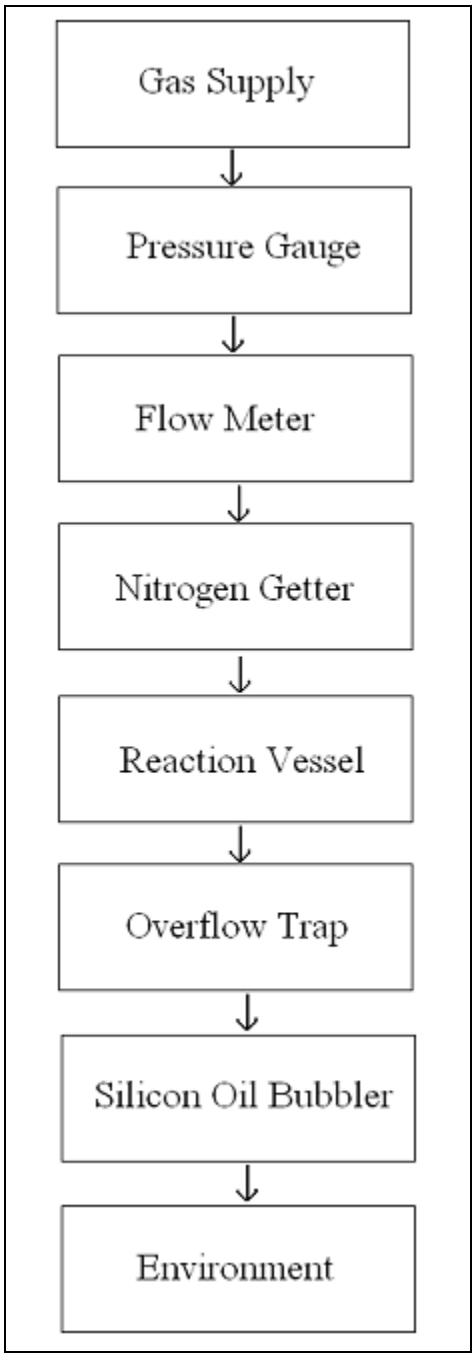

Figure 2. Schematic of process gas flow path.

(see Section 4). The gas supply is controlled via a gas flow meter (Dwyer model number RMB-50-SSV) and a pressure gage (Dwyer model number 2030). There is then an inline 5 psi relief valve (Swagelok model number SS-4C-5). This is to avoid over-pressurization of the system and is located immediately before the titanium sponge getter. The getter was designed, manufactured and installed in this position after experiment 57 as part of this project. For experiments 53-57, it was located between the gas cylinders and the flow meter. It was moved to its final downstream position to account for any leaks or sources of contamination introduced by the flow meter, pressure gage, or pressure relief valve.

Once the gas leaves the getter in this final configuration, it flows directly into the reaction vessel through an inlet valve. The process and purge gas is heated as it enters the reaction vessel through a copper coil inside of the reaction vessel. The gas exits the copper coil at the end of the vessel near the metal sample, passes over the sample, and then flows out of the reaction vessel through an outlet valve. After leaving the reaction vessel, the gas passes through an overflow trap followed by a silicon oil bubbler to prevent any contaminating gasses from entering the system. The gas then travels through a PVC tube to a fume hood, where it is vented to the atmosphere.

3.1.2 Reaction Vessel

The reaction vessel and its internal parts are shown in Figure 3. The reaction vessel is a 2-in outer diameter aluminum oxide tube, sealed with a stainless steel tube seal via rubber gasket. The tube seal, inlet gas line with the copper inlet coil, outlet gas line, stainless steel heat shields, and K-type thermocouple are all one unit that can be inserted and removed from the reaction vessel together. The interface of the inlet gas line, outlet gas line, and thermocouple with the tube seal, were all sealed using an epoxy designed for vacuum conditions. The samples are contained in an alumina crucible which is held in place within the reaction vessel by a stainless steel sample tray.

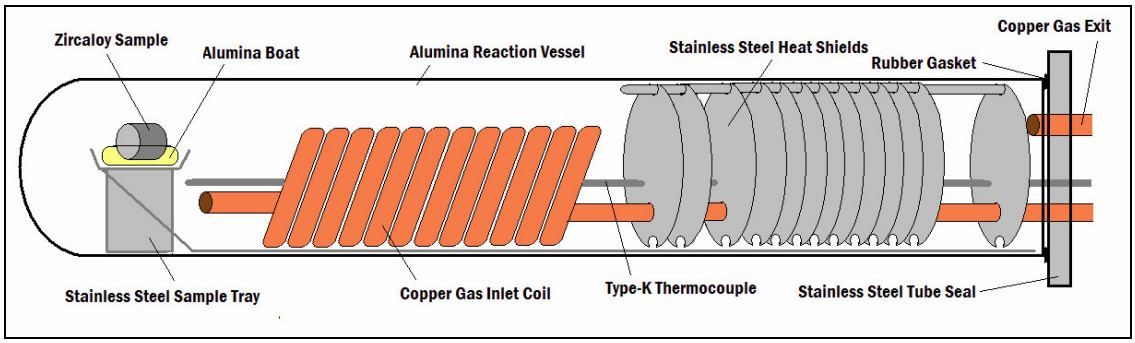

Figure 3. Schematic of reaction vessel. [3]

The gas enters the reaction vessel via the inlet tube, which then flows through a coil of copper tubing prior to being passed over the sample. This insures that the temperature of the process gas is at thermal equilibrium with the sample before the sample exposure to fresh hydrogen takes place.

3.1.3 Titanium Sponge Getter

The getter was added to the system after experiment 52 in order to remove contaminants, most notably nitrogen, oxygen, and water, from the gas source as well as contaminants introduced due to possible leaks in the system. The getter consists of a 1-5/8 inch outer diameter aluminum oxide tube with a 350 W furnace (Watlow model number VC401N06A) placed around it. The tube was filled with titanium sponge in such a way that the sponge is only in the heated region of the tube. It is important that the titanium sponge remain only in the heated region in order to avoid hydriding the titanium, which would reduce, or perhaps even eliminate, the hydrogen actually reaching the sample.

For this reason a titanium cage was created to contain the titanium sponge. The cage was created using three titanium rods to connect two custom-made perforated titanium plates. The rods were connected to the plates using titanium screws. The furnace around the getter is maintained to achieve an internal temperature of 1000°C to 1100°C. This prevented the titanium from reacting with the hydrogen, but allowed it to rapidly consume any oxygen, nitrogen, and water which might be in the system. It is essential that the getter remain at temperature with gas flow at all times, even when there is not a sample in the reaction vessel. This is because of the length of time it takes to heat up as well as the desire to maintain a pure getter system.

3.2 Experimental Procedure

3.2.1 Sample Preparation and Loading

The first step in the experimental process is to prepare the samples. The samples began as nuclear grade Zircaloy-4 tubes 5-in long with an inner diameter of 0.515-in and an outer diameter of 0.580-in. The tubes were then sectioned into small cylinders of approximate length 0.6-in and approximate mass 3.5 grams, using a Leco diamond saw model number VC-50. The sectioned samples were then cleaned in ethanol in an ultrasonic cleaner.

A typical experiment begins by obtaining an accurate mass measurement of the sectioned Zircaloy-4 sample to within 0.0001 grams using a precision balance (Metler Toledo model number AB104-S) installed inside of an inert argon atmosphere glovebox. First, the sample is weighed along with the alumina crucible. Next, the sample is removed and the mass of the alumina crucible is obtained. Finally, the scale is zeroed with the alumina crucible on it, and the mass of the sample is measured directly. This method is used for two reasons. First, the separate masses of the sample and alumina crucible are compared to the mass of the masses of the two together. This is to insure that accurate masses are recorded. For quality control reasons the masses were not recorded unless they agreed to within 0.0003 grams. If they did not agree to 0.0003 grams, the mass measurements were repeated until this criterion was met. The other reason this weighing process was implemented is because the mass of the sample alone is needed in order to calculate the “percent hydride”, a term used to reflect the quantity of zirconium hydride formation after the experiment. The masses of the sample and the

alumina crucible together before and after the reaction are compared to compute the mass change (Δm). This Δm is then applied to the mass of the sample alone in order to determine the percent hydride (P_H) formed during the test by Equation 4.

$$P_H = \frac{\Delta m}{m_{Z-4}} \times \frac{M_{Z-4}}{M_H} \times \frac{1}{2} \times 100$$

P_H = Percent hydride
Δm = Mass difference before and after reactoin
$m_{Z\text{-}4}$ = Initial mass of sample
$M_{Z\text{-}4}$ = Effective atomic mass of Zircaloy - 4
M_H = Atomic mass of hydrogen [4]

The Zircaloy sample and alumina crucible are then placed on the stainless steel sample tray shown in Figure 3, and inserted into the reaction vessel. The stainless steel tube seal assembly with attached tubing, heat shields, and thermocouple is then carefully inserted into the aluminum oxide tube making sure that the sample remains upright during loading. The tube is then sealed by hand tightening three wing nuts and removed from the glovebox by way of the airlock.

3.2.2 Furnace Loading and Hydride Reaction

Once the sample has been weighed and loaded into the reaction vessel, it is then inserted into the furnace (Astro Industries model number A143S). The outlet tube is connected first, followed by the inlet line. When both the outlet and inlet lines are connected, the inlet valve is opened followed by the outlet valve. This seemingly tedious procedure is performed in order to avoid over-pressurization of the system, as well as to minimize any possible contaminates which may enter the system. Over-

pressurization was a concern because, as stated previously, the purge gas was never turned off once the titanium sponge getter was added.

The system is then brought to the approximate operating pressure and flow rate of 25-in of H_2O and 3 standard cubic feet per hour (SCFH) and the variable voltage transformer (Staco Energy transformer model number 3PN1510B) used to control the furnace is turned up to 80% (100% = 120VAC). The reason that the pressure and flow rate are brought to operational values during heating is because it was found that if they were not, the extra flow rate would have a cooling effect on the reaction vessel, causing temperature instability. The higher pressure also functions to minimize any gaseous impurities which may enter the system.

A calibration curve was produced using temperature data from the early experiments, which indicates when the transformer should be turned down from 80% to the desired operating value. This plot is shown as Figure 4. Once the temperature reaches the value determined from Figure 4, the transformer is turned down to the operating voltage. This was done in order to maximize temperature stability throughout the experiment. In order to maintain consistent temperature values from experiment to experiment, the transformer setting is set based on its output voltage in experiments including and after number 68 instead of visual inspection of the transformer dial as was performed in experiments prior to 68. The voltage settings were found by first visually setting the transformer to the desired setting and then recording the voltage. This insured that for any future experiments performed at this temperature, the transformer would be at a consistent voltage. This was done due to the difficulty in achieving

consistent transformer settings by visual means. It also allows for the possible use of a backup transformer which may not be calibrated exactly the same. This proved useful when the transformer used in this experiment failed and had to be replaced by an identical Staco Energy transformer with slight differences in calibration.

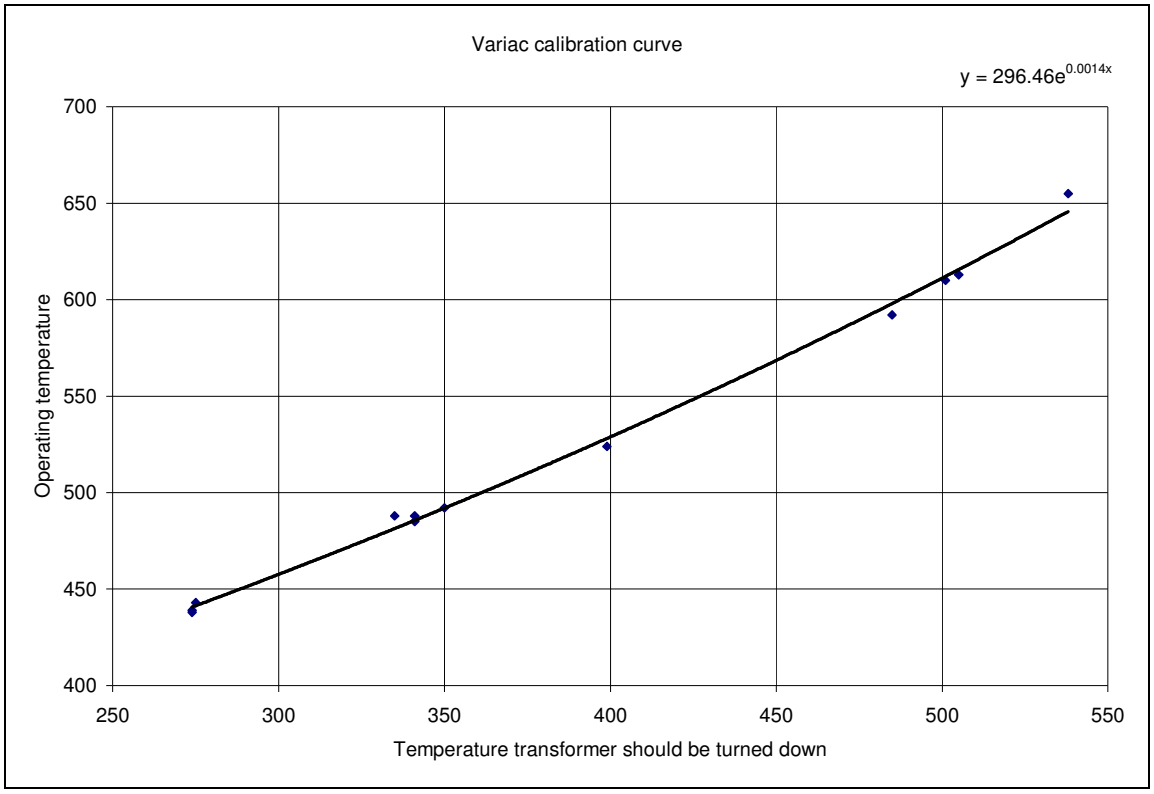

Figure 4. Plot showing when to set transformer to operating voltage.

Once the transformer is set to the desired setting, the temperature is allowed to come to a relatively steady state of +/- 0.2°C per minute. At this point the Ar-5%H_2 gas flow is started, the UHP argon flow is stopped, and the current time and temperature are noted. The flow rate is set to 3 SCFH and the pressure is set to 26.5-in H_2O. These

variables are set by adjusting the valve immediately after the regulator as well as the outlet valve of the reaction vessel. This gives control over both flow rate and pressure. The gage pressure of 26.5-in H_2O corresponds to a process pressure of 25-in H_2O because a 1.5" of H_2O pressure drop was measured across the titanium getter for a flow rate of 3 SCFH.

3.2.3 Process Shutdown and Furnace Unloading

After the desired reaction time has been accomplished, the furnace is shut down, Ar-5%H_2 gas flow is stopped, and UHP argon gas flow is started. It then becomes desirable to decrease the flow rate through the process vessel to conserve gas. The pressure is maintained at 26.5-in H_2O, but the flow rate is reduced to the point where ~4-5 bubbles per second are observed in the bubbler at the exhaust point. The pressure must remain high to minimize contaminants in the system, but at this point in the process the effect due to flow rate is minimal. The reaction chamber is then cooled until it reaches a temperature of no more than 40°C. The value of 40°C was chosen because it is below the temperature where any appreciable reactions with air should occur, and is at a point where the reaction vessel can be handled safely without a risk of being burned. The rate of cooling is approximated by Equation 5 and can last anywhere from 10 to 12 hours depending on the final process temperature. Where T is the system temperature, T_o is the temperature that the system was turned off, and t is the time after system shutdown in minutes.

$$T = T_o e^{-0.0038t} \qquad [5]$$

When the reaction chamber reaches an appropriately low temperature, the outlet valve is closed, followed by the inlet valve. The inlet tube is then disconnected followed by the outlet tube. Similar to the reasons stated above, the process is performed in this order to minimize contaminants as well as to avoid over-pressurizing the system.

3.2.4 Sample Analysis

The reaction vessel is removed from the furnace and placed into the glovebox, where it is opened and the sample is carefully removed. The alumina crucible which contains the sample is weighed on the scale and the combined mass is recorded. This combined mass is what is then compared to the pre-reaction mass in order to determine the percent hydride from Equation 4.

4. RESULTS

As cited in Section 2.2, the basic setup for this hydride formation study experiment was established by D.T. Kraemer [3], who performed fourteen proof-of-concept experiments using the original system configuration at Purdue University. The original experiments did not lay out a systematic test matrix to evaluate hydride formation, but rather they scoped out the behavioral boundaries for several process variables. The work reported here picks up where that work ended and another eighty seven experiments have been carried out. Appendix A provides a detailed summary table for all 101 experiments. Experiments 15 to 19 (Section 4.1) established the impact of pressure and sample orientation on hydride formation in Zircaloy-4. Experiments 20 to 24 (Section 4.2.1) studied the temperature dependence of hydride formation. Experiments 26 to 29 (Section 4.2.2) attempted to show the effect of the physical integrity of zirconium hydride near the alpha-beta eutectoid temperature. Experiments 30 to 57 (Section 4.2.3) focused on determining the source of nitrogen contamination, and to demonstrate that the nitrogen contamination had been minimized. Experiments 32, 45, and 96 (Section 4.2.3) were control experiments performed in an effort to quantify the amount of contamination in the system. Experiments 58 to 101 (Section 4.3) were performed to study the temperature and time dependence on the rate of hydrogen pickup in Zircaloy-4 tubes. The results for each of these tests are reviewed in the following sections.

(Experiments 15 to 47 were performed at Purdue University when the author was enrolled as a dual-status graduate-undergraduate student. The author and his advisor moved this project to Texas A&M University where the system was rebuilt and experiments 47 to 101 were performed.)

4.1 Effects of System Pressure on the Hydride of Zircaloy-4

The process gas pressure in Kraemer's experiments (samples 1 to 14) ranged from 4.5 to 28-in H_2O. In an effort to eliminate pressure as a process variable, experiments 15 to 19 were performed to determine what effect, if any, the cover gas pressure might have on the zirconium hydride formation reaction. It is known that near atmospheric pressure the solubility of hydrogen in zirconium is nearly independent of pressure for the temperatures of interest, and can be seen in Figure 5. [7] However, very few of the experiments performed for this thesis were allowed to go to completion. While the theoretical hydrogen content may be independent of pressure, the reaction rate may still be pressure dependent.

This was found to be the case and data supporting this conclusion are tabulated in Table 2 and illustrated in Figure 6. Experiment 16 was excluded from this plot because it was dropped on the glovebox floor prior to weighing, so the P_H measurement was not reliable. The experiments were performed at 10.5 and 25-in H_2O and held at ~520ºC for ~6 hours. The results clearly revealed that the rate of hydride formation was more rapid for higher cover gas pressures. Due to the strong direct correlation between pressure and the hydride formation rate, it was decided to standardize the system pressure to 25-in H_2O for all remaining experiments. The higher pressure was chosen for all experiments

after Exp. 19 for the simple fact that the reaction rates will be higher, thus decreasing the amount of time required for each experiment.

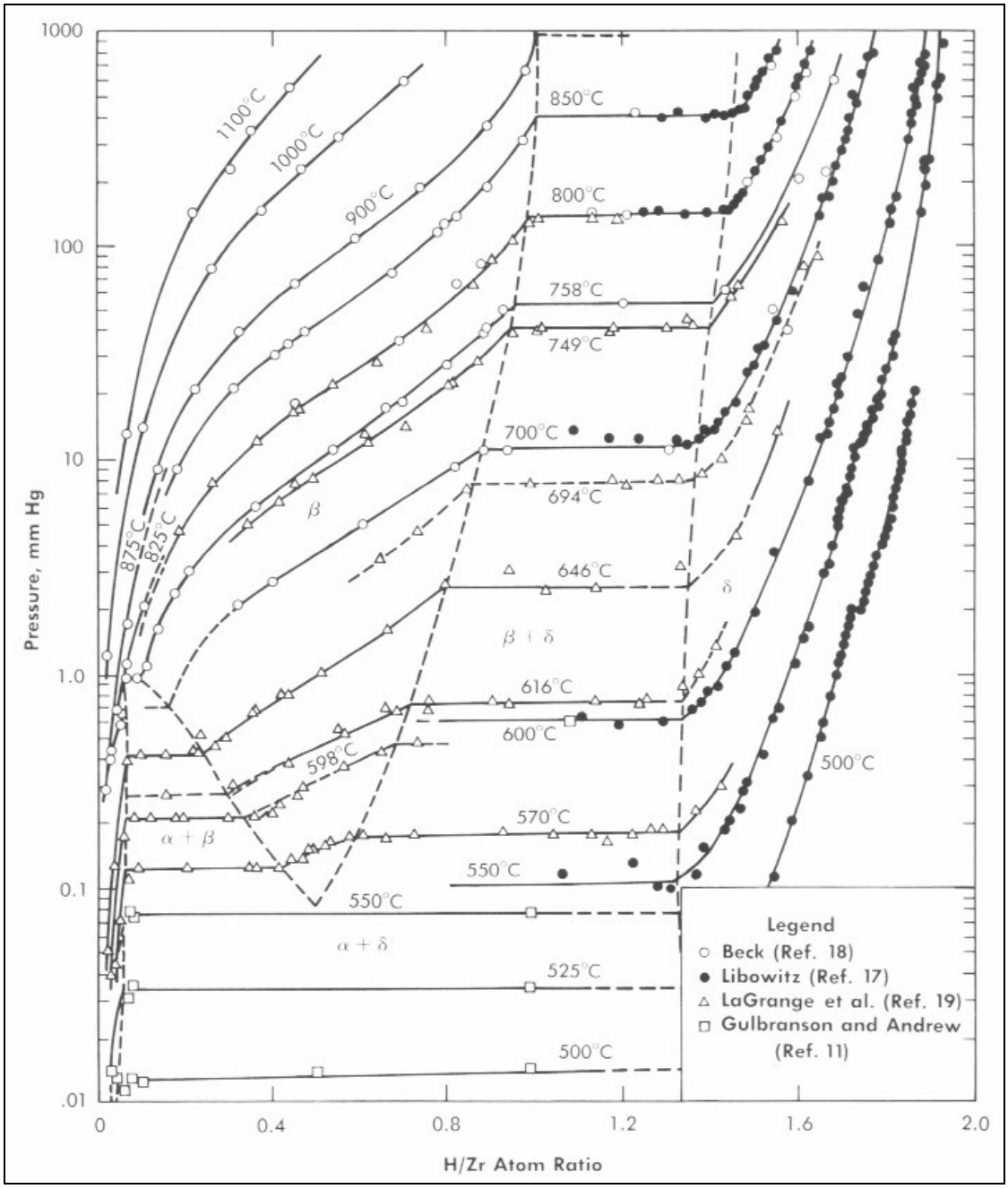

Figure 5. Hydrogen pickup as a function of temperature and pressure. [10]

In addition to the pressure differences, the sample orientation was briefly studied. In other words, the orientation of the Zircaloy tube was varied from horizontal (i.e., on its side) to vertical (i.e., upright). The reasoning for the variation was suggested by the results from Kraemer's tests that showed an asymmetric distribution of hydride formation in the horizontal orientation; that is, the top wall of the tube hydrides more rapidly than the bottom. The results from experiments 15 to 19 are also highlighted in Figure 6. While the results seem to indicate a slightly higher hydrogen pickup for the upright orientation, this brief study was not sufficient to come to any conclusion based on sample orientation. Even so, every sample after experiment 19 was loaded into the process vessel in an upright position.

Table 2. Tabulated results of orientation/pressure study.

Exp.	Orientation	Pressure in-H_2O	P_H
15	upright	10.5	18
16	side	10.5	11
17	upright	24.75	92
18	side	24.75	65
19	side	10.5	11

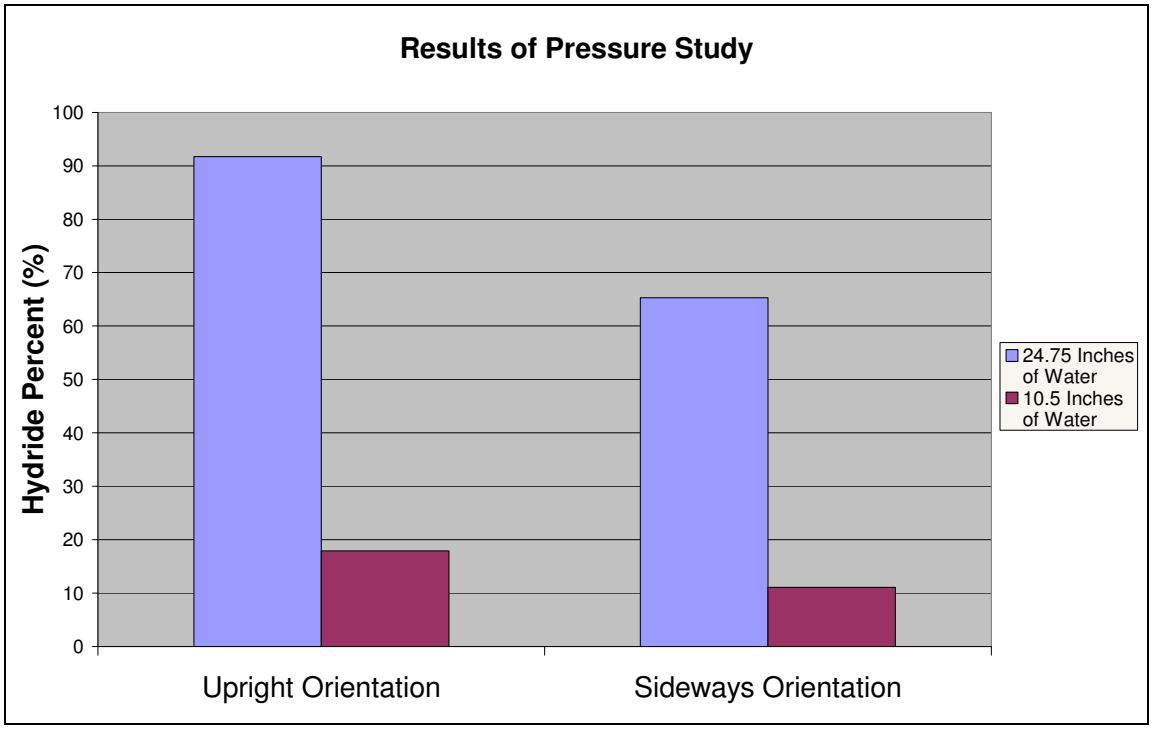

Figure 6. Plot indicating effect of pressure on hydride rate.

Prior to experiment 53 (before the getter system was added) the system pressure would remain very nearly constant during experimental runs with very little fluctuation. However, during and after experiment 53 the pressure would fluctuate. The observed fluctuation was manifested as a slow increase in pressure corresponding to when the gas flowing through the system was switched from argon to the Ar-5%H_2 mixture as discussed in section 3.2.2. This seems to imply that there is some sort of flow restriction being created when the Ar-5%H_2 gas mixture enters the getter. It is hypothesized that the flow restriction might be caused by hydride formation in the titanium sponge, but this was never verified because it was outside of the scope of this project.

This issue was handled by manually adjusting the pressure as needed in order to maintain a pressure of 25-in H_2O. It is recommended that if this experiment is to be repeated, a precise low pressure regulator be installed in the system. This would make the process much less labor intensive, but more importantly, increase the reliability of the data. The process of manually adjusting the pressure caused variations of +/- 3-in H_2O or +/- 0.1% absolute pressure.

4.2 Discovery and Removal of Process Gas Contamination

4.2.1 Dependence of Hydride Formation on Temperature

Experiments 20 to 24 were designed to gain preliminary understanding on hydride formation as a function of temperature. Each sample was hydrided for six hours with the exception of experiment 24 which was hydrided for 7 hours, and the temperatures varied from 353°C to 747°C. The results from these tests are summarized in Table 3 and are plotted in Figure 7.

Table 3. Tabulated results of temperature study at six hours.

Exp.	°C	P_H
20	353	6
21	451	6
22	541	5
23	647	15
24	747	48

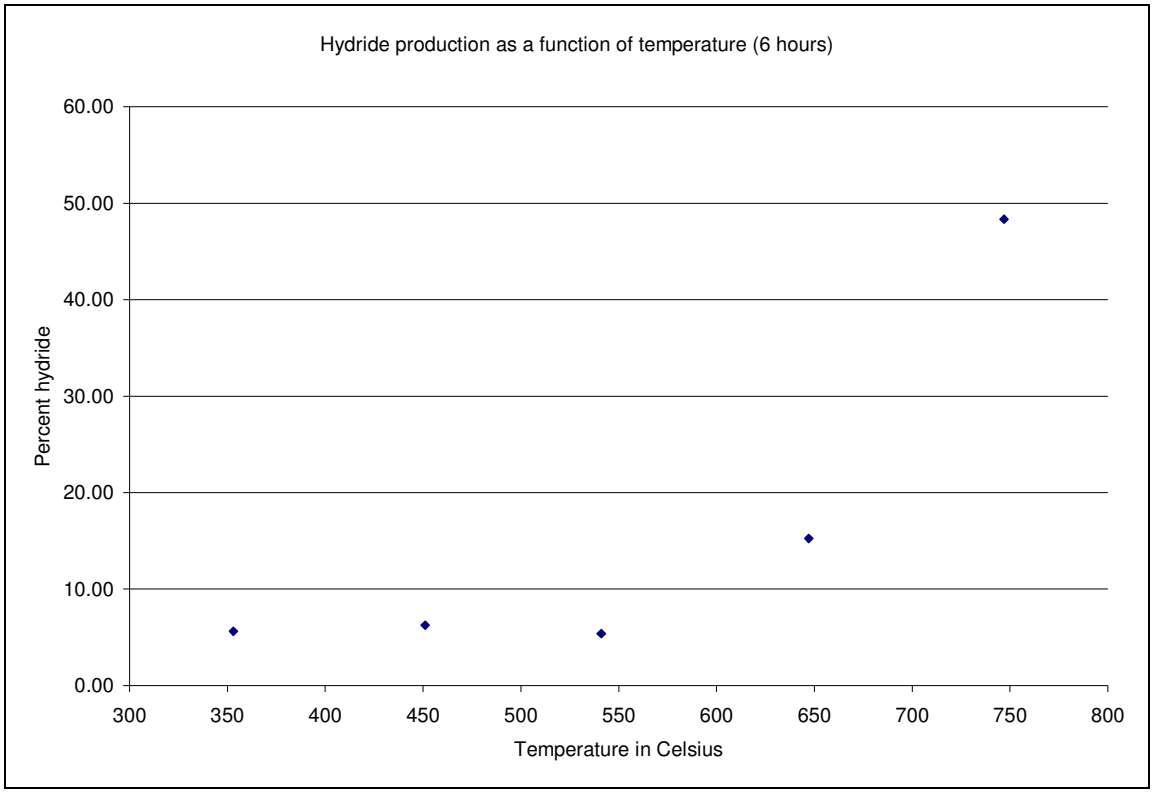

Figure 7. Results from 6 hour temperature study.

The above data was initially puzzling because of the inconsistent results, especially when compared to later experiments. Experiments 20 to 22 showed abnormally low hydride percentages that were within the same range as the control experiments (discussed in section 4.2.3). However the most important discovery from this data came from experiment 24. The sample was removed from the process vessel and was observed to have a significant gold color. Pictures of experiment 24 are show in Figure 8. There is very good reason to believe that this gold color was due to reaction with nitrogen impurities in the cover gas, thus creating zirconium nitride. It is known that the rate at which nitrogen is absorbed in zirconium greatly increases at temperatures

above 700°C. [7] This would explain why experiment 24 showed a strong indication (i.e., gold discoloration) of the presence of zirconium nitride while the samples from experiments 20 to 23 did not. Based on this hypothesis it was determined that the system gas supply was not as pristine as once thought. Due to the probability of nitrogen contamination in the system, these experiments are not included in the final rate study.

Figure 8. Golden color of experiment 24 indicating nitride contamination.

4.2.2 Hydride Formation at Temperatures near α-β-δ Eutectoid Temperature

The next five experiments (nos. 26 to 29) were designed to study the effects of hydride formation at temperatures near the α-β-δ eutectoid temperature. These experiments were all performed for six hours. It was postulated that if the temperature was held near the α-β-δ eutectoid temperature, the material would more easily turn to powder due to the phase change between the alpha and beta phases. While the concept of phase changes within the material turning it to powder remains just as true, the results

from experiments 26 to 29 were wildly inconsistent, in part because of the system contamination noted in the previous section. The data from these experiments is shown in Table 4.

Table 4. Results of study for temperatures near α-β-δ eutectoid temperature at six hours.

Exp.	°C	P_H
26	547	85
27	543	59
28	543	44
29	542	24

These experiments showed that the system was not at a point where reproducible data could be obtained. This is apparent due to the fact that these four experiments varied in temperature by only 5°C, yet varied in hydride percent by up to 60%. This gave a clear indication that either the experimental setup or the experimental process needed to be changed.

4.2.3 Discovery of Sources of Nitrogen Contamination and Their Removal

The data from experiments 26 to 29 made it clear that more work needed to be done to increase the reliability of the data produced by the system. Experiments 30 to 52 represent a sequence of troubleshooting experiments designed to discover the cause of the inconsistencies in the data due to nitrogen contamination. One interesting result from these experiments came in experiment 31. This experiment showed a mass gain which corresponded to a theoretical percent hydride of $P_H = 107.4\%$. This result could indicate that the sample contained pure ZrH_2 with excess hydrogen in solution, but that

is unlikely. The more likely scenario however is that this data represents a false hydrogen pickup and that contaminating elements such as nitrogen, oxygen, and water are responsible for such a high apparent hydride. The reason that this appeared to be the more likely scenario is because nitrogen contamination was suspected based on the results described above and because the P_H is determined by a change in mass. For each contaminating atom of oxygen or nitrogen, a false hydrogen pickup of 16 or 14 atoms respectively is observed. This illustrates that it is absolutely necessary to eliminate any contamination from the system.

Experiments 32, 45, and 96 were control experiments intended to give a quantitative measure of contamination within the system. The control experiments were performed in exactly the same manner as the hydride experiments, with the exception that a flow of Ar-5%H_2 gas is never passed over the samples. A summary of these experiments is given in Table 5. The results from experiments 32 and 45 show a high false hydrogen pickup due to contamination. Experiment 96 is shown here for comparison, but it was run after the contamination was eliminated from the process gas, as described later in this section. A fundamental flaw in performing control experiments for this particular setup is that during the hydride formation, the samples crumble and a high surface area is created. This greatly increased surface area increases the rate of hydrogen pickup, but it also should increase the pickup of any impurities which may be in the system. The control experiments lack this increase in surface area, so any indicated false hydrogen pickup is not conservative, but instead should under predict the

actual level of contamination. This is the reason that control experiments did not play a larger role in this project.

Table 5. Tabulated results for control experiments.

Exp.	°C	Time in hours	P_H
32	519	26	4
45	567	21	6
96	440	4	0

As stated previously experiments 30 to 36 were performed to determine the reason that the hydride results were inconsistent. During these experiments the purity of the Ar-5%H_2 gas supply was called into question but it was not until after experiment 36 that the true cause of contamination was discovered. After experiment 36 it was discovered that the one psi relief valve installed in the system was leaking. This valve is designed to allow gas flow in one direction and only when the pressure of the system exceeds one psi. It was found that this valve was allowing a small amount of gas through even when the pressure was under one psi. This indicated that the valve was faulty and pointed to the very real possibility that if the valve let gas out at pressures less than one psi, it was also allowing air into the system. This explained the appearance of gold nitride in the samples, and hence a major cause of inconsistencies within the experimental results. This one psi valve was replaced with a functioning five psi relief valve.

Because the relief valve had been replaces and was known to be one of the sources of nitrogen contamination, experiments 37 to 57 were performed in an effort to

acquire valid reproducible data. However, the data from experiments 37 to 39 were questionable to various degrees and for various reasons. Experiment 37 showed an abnormally low hydrogen pickup, experiment 38 had an anomalous temperature instability such that the temperature was allowed to cross the alpha-beta eutectoid temperature in a poorly controlled manner, and Ar-5%H_2 gas flow stopped an hour prior to the completion of experiment 39. The errors in experiments 37 to 39 were due to operator error instead of error caused by nitrogen contamination.

Therefore, the data from experiments 40 to 57 represent the first step toward a systematic study of the hydride formation process and the results were generally very good. They displayed very high values of P_H and more importantly were consistent with expected results as shown in Table 6. The data shows that times on the order of 6 to 24 hours are not necessary for the samples used in this study, and in fact are not even desirable. This is because high P_H values (approaching 90 to 100%) were routinely produced beyond six hours.

While these experiments showed predictability in the data, there was still some visual observation of slight nitrogen contamination. Perhaps the most peculiar result from experiments 40 to 57 was the appearance of experiment 46 (Fig. 9). When the specimen was removed from the reaction vessel, it was found to be completely deteriorated into shards and small pieces and it had a brown coloration. This deterioration and discoloration gave the sample an appearance similar to dried tobacco. The result of experiment 46 which was performed at 310 ºC for 24 hours, is shown in Figure 9 and can be compared to a picture of experiment 47 which was performed for 24

hours as well at 432ºC in Figure 10. It is possible that the appearance of experiment 46 is the result of the low temperature, but this was never reproduced. While experiment 46 was brown in color, it did not have the same luster as the experiments which showed a clear indication of nitrogen contamination. The brown color was also considerably different from the gold color indicative of zirconium nitride which gives the impression that this may not be a nitrogen contaminated specimen. This conclusion is supported by the fact that the zirconium-nitrogen reaction is very slow at 310 ºC.

All experiments up to experiment 47 were performed at Purdue University. After this the entire experimental apparatus was relocated to Texas A&M University where experiments were continued. The entire system was broken down, cleaned with alcohol, resealed, and then rebuilt (with some improvements) after its relocation.

Table 6. Results for experiments 40-57.

Exp.	°C	Time in hours	P_H
40	582	24	90
41	556	24	97
42	570	6	84
43	570	18	97
44	563	12	91
45	567	21	6
46	310	24	57
47	432	24	86
48	572	6	72
49	566	6	78
50	566	6	53
51	565	6	17
52	571	6	21
53	574	6	90
54	575	6	92
55	567	4	35
56	576	4	72
57	579	4	46

*Exp. 45 was a control experiment

Figure 9. Experiment 46 showing tobacco-like appearance.

Figure 10. Experiment 47 for comparison with experiment 46.

While experiments 40 to 50 seemed to show reliable results, there was still a slight visual indication of nitrogen contamination. For this reason, UHP argon was used as the purge gas for all experiments after experiment 51 and it was decided that the system would further benefit from the addition of a nitrogen getter. This titanium sponge getter as described in section 3.1.3 was put into place after experiment 52. The purpose of adding a getter to the system was to remove impurities from the process gas. It was eventually determined (after experiment 57) that the system performs better if the getter were relocated to a position in the gas flow path which was immediately before the reaction vessel. This would guarantee that any contaminates which may leak into the system through the various seals and instruments are removed prior to entering the reaction vessel. All seals and connection fittings were either wrapped in Teflon tape or sealed with Room Temperature Vulcanizing (RTV) silicon. The combination of using UHP argon, installation of the nitrogen getter, and improving the seals, completely eliminated any observable trace of nitrogen or oxygen contamination. It can be concluded from these results that the hydride reaction is strongly affected by nitrogen, oxygen, and water contamination which may be in the system.

4.3 X-Ray Diffraction Analysis

An X-Ray Diffraction (XRD) analysis was performed on samples 31, 40, 43, and 46, as shown in Figures 11, 12, 13, and 14 respectively. The analysis of sample number 31 agrees very well to epsilon phase zirconium hydride meaning that it is very probable that the actual composition is at least 85% zirconium hydride with the remaining weight gain caused by impurities. This is the sample which had a calculated P_H value of

107.4%. In the figures below, there is often a slight shift in the higher angle spectral peaks, which is typically accompanied with irregular sample preparation and "out-of-plane" powder loading. These shifts were acceptable in this study since there was no need to optimize the powder loading for analytical results; sample identification is all that was sought.

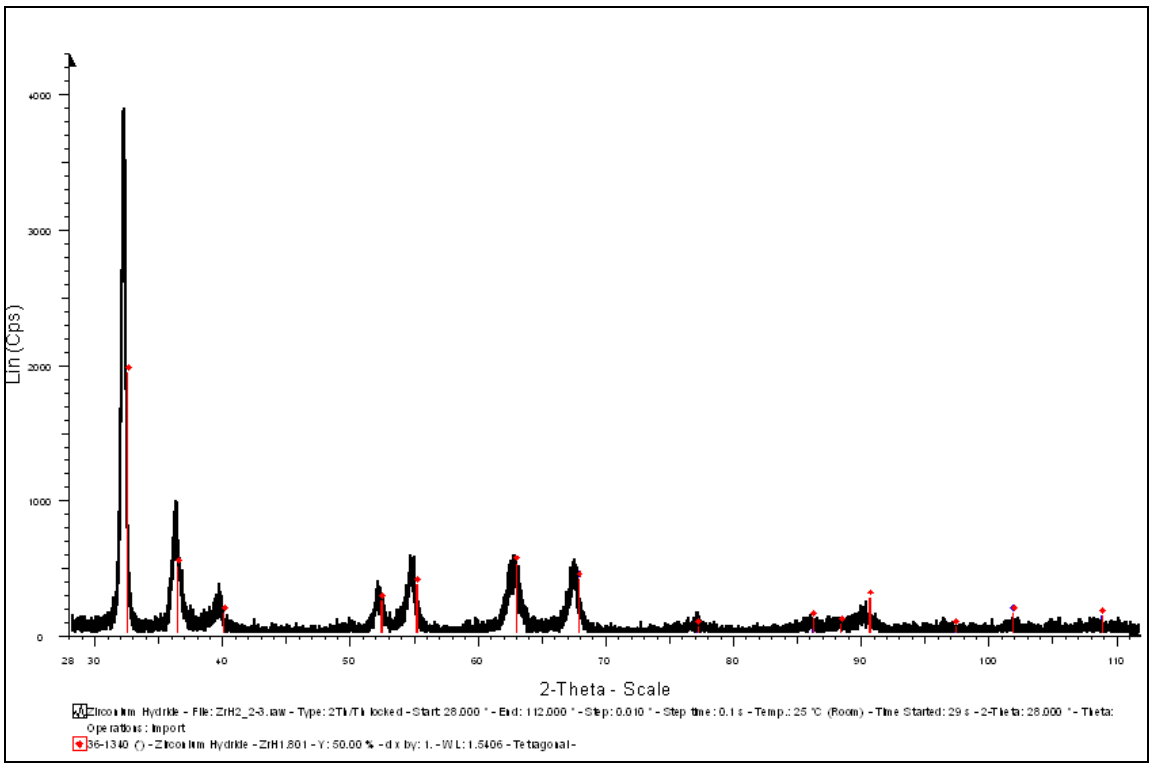

Figure 11. XRD analysis of experiment 31 showing clear indication of epsilon phase zirconium hydride.

The XRD peaks for experiment 40 also showed a clear indication of the presence of zirconium hydride (Figure 12). The spectrum produced was very clean but showed

some small peaks which were unaccounted for. These peaks could be due to the presence of tin or tin compounds because Zircaloy-4 is composed of 1.2-1.7% tin as shown in Table 1. Another possible cause might be from nitride formation within the material. They could also be caused by the presence of various phases of zirconium hydride coupled with the somewhat low confidence level of the XRD software's fitting program due to its limited data set. This is the more likely scenario because it is difficult to produce visible results for species with low concentrations such as tin in Zircaloy-4 using XRD.

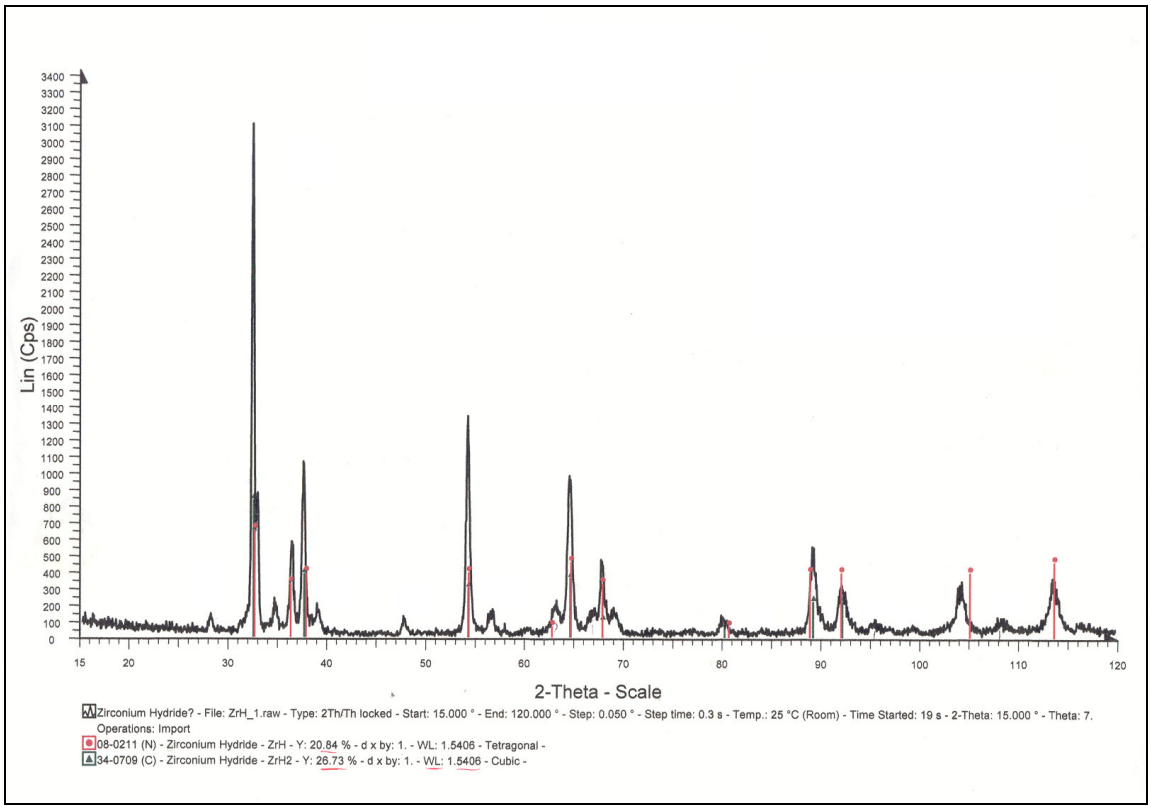

Figure 12. XRD analysis of experiment 40 showing indication of zirconium hydride.

The plot for experiment 43 showed results that indicated the presence of zirconium hydride, but was very noisy as shown in Figure 13. The major peaks corresponded to the presence of zirconium hydride but it was very difficult to get any usable results from any smaller peaks. The reason that the spectrum was so noisy is because of the low number of counts collected by the XRD machine. These low counts were not enough to clearly distinguish some of the smaller peaks from the background.

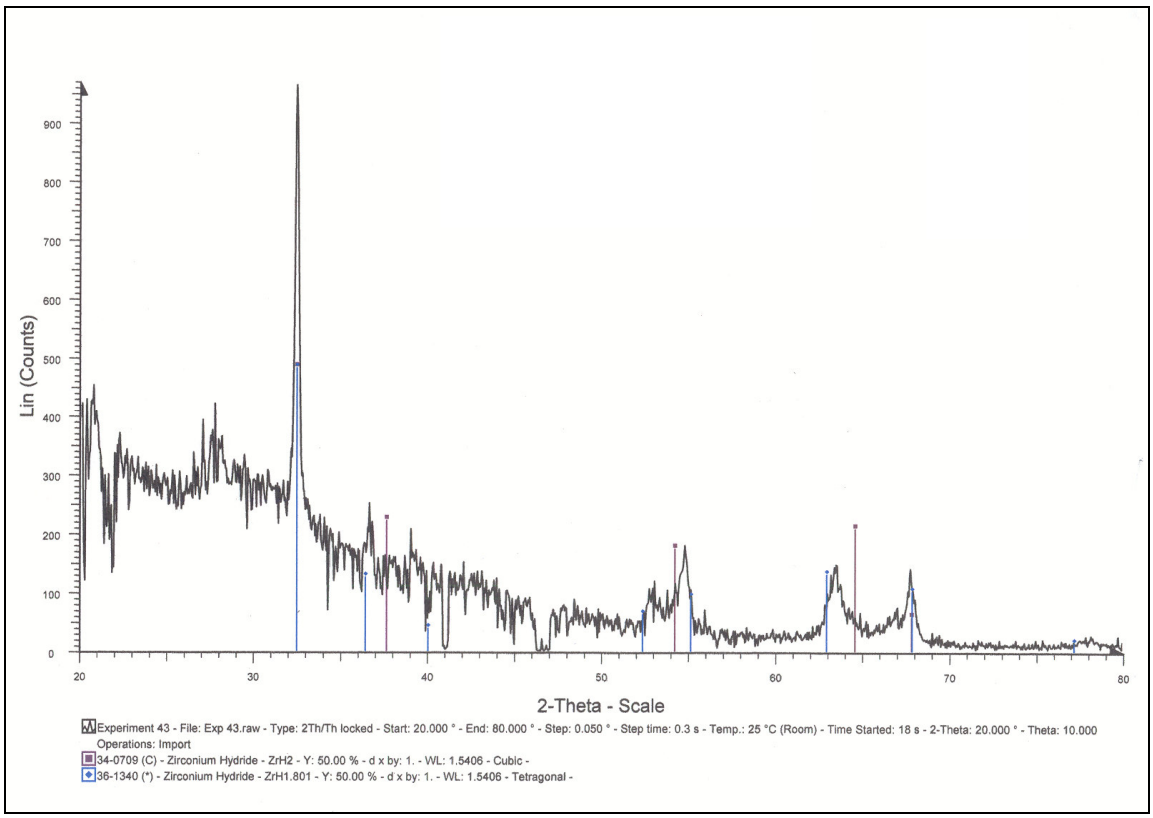

Figure 13. XRD analysis of experiment 43 showing indication of zirconium hydride.

The spectrum shown in Figure 14 shows the results of the XRD analysis of experiment 46. This spectrum indicates the presence of zirconium hydride. As with the

previous patterns it is difficult to determine anything else about the composition of the samples simply because it is difficult to see the presence of species which have low concentrations in the sample using XRD.

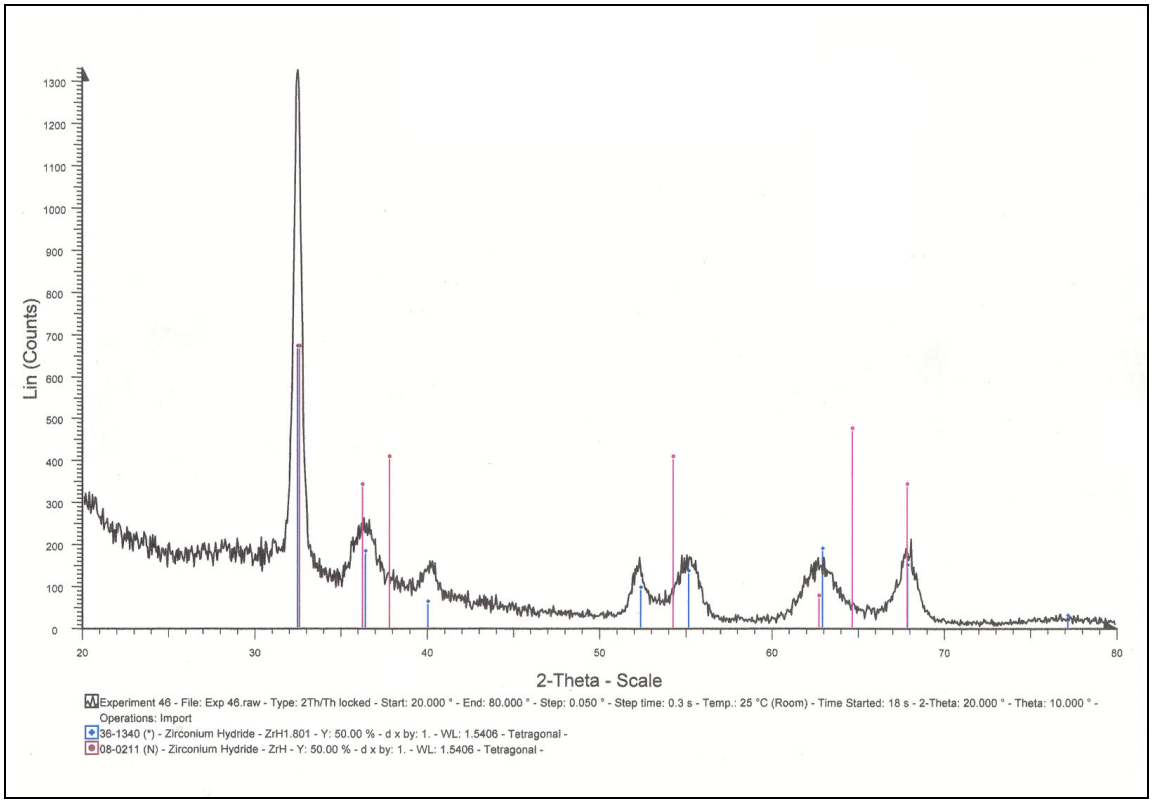

Figure 14. XRD analysis of experiment 46 showing indication of zirconium hydride.

It was determined from the XRD analyses that zirconium hydride was in fact being produced. It was also observed, as expected, that XRD is not necessarily a useful tool for determining the presence of any other chemical species. For this reason, XRD analysis was no longer performed after experiment 46.

4.3 Rate Study on the Formation of Zirconium Hydride as a Function of Time and Temperature

The results obtained from experiments 15 to 57 gave an indication as to how the system needed to be changed in order to achieve reproducible data. The most notable of these results was the elimination of contaminating gasses such as nitrogen from the process gas. At this point, it finally became possible to acquire the desired data to evaluate the time and temperature dependence of hydride formation in Zircaloy-4.

This rate study was performed using three times (1, 2, and 4 hours) and six temperatures (440, 480, 520, 560, 600, and 640ºC). The three times were chosen largely based on the results from experiments 40 to 57, which showed that hydride times beyond six hours would produce P_H levels above 90%. Therefore, these short time periods were chosen so that a broad range of P_H data would be obtained to quantify the formation process as it progresses instead of only at high P_H levels. The six temperatures were chosen such that three of them were above the α-β-δ eutectoid temperature (540ºC) and three were below this point.

Duplicate experiments from this text matrix (plus a few repeat experiments) were completed with experiments 58 to 101, with experiment 96 being a control sample. Table 7 shows a summary of the data from these tests and the results are presented graphically in Figure 15. Duplicate experiments were performed to show systematic reproducibility and to better approximate the true behavior. In theory, multiple experiments (five or more) at each time-temperature combination would improve the

data statistics, but the selection of two experiments each was reasonable to show reproducibility and to assure the timely completion of the project.

As expected, the rate of hydride formation varies strongly with temperature in the first four hours of the process. The only exceptions to this observation can be seen in the four hour tests. These four hour experiments displayed a slight decrease in hydrogen pickup for temperatures of 600 and 640ºC. This is presumed to be caused by the samples reaching their maximum hydrogen content and this actually indicates a leveling off of the hydrogen pickup. This would also indicate that Zircaloy-4 rapidly reaches its maximum hydrogen content at temperatures around 450ºC.

It was expected that the hydride formation data would behave differently when the sample was held above and below the α-β-δ eutectoid temperature and this was indeed the case. It was observed that samples which were hydrided at temperatures below 540ºC became highly embrittled and were often reduced to shards after the hydride reaction. At temperatures above 540ºC, the samples were often entirely intact after the experiment, even though the P_H values were high. All experiments produced an embrittled sample which could be ground to a powder. The difference is that for temperatures below the eutectoid line, the sample had already begun disassembling itself and was dramatically easier to grind into a very fine powder. Experiments performed at temperatures above the eutectoid line, for the most part remained intact upon the completion of the hydride reaction and the samples required much more effort to grind into a powder.

Table 7. Experimental results from rate study.

Exp.	ºC	Time in hours	P_H
58	568	4	94
59	568	4	95
60	519	4	92
61	520	4	93
62	481	4	78
63	485	4	80
64	481	4	94
65	569	1	43
66	579	1	21
67	600	1	30
68	479	4	78
69	435	4	79
70	436	1	1
71	522	1	8
72	440	4	42
73	526	2	26
74	422	1	12
75	441	1	2
76	436	2	1
77	530	2	33
78	611	4	88
79	616	1	36
80	614	4	83
81	576	2	49
82	654	4	86
83	648	4	87
84	578	2	49
85	665	2	87
86	643	2	71
87	613	2	72
88	615	2	57
89	537	1	7
90	635	1	34
91	487	1	4
92	636	1	31
93	477	2	62
94	475	2	64
95	482	1	14
96	440	4	0

Table 7. Continued.

97	429	2	14
98	558	1	31
99	483	2	25
100	427	2	31
101	474	2	15

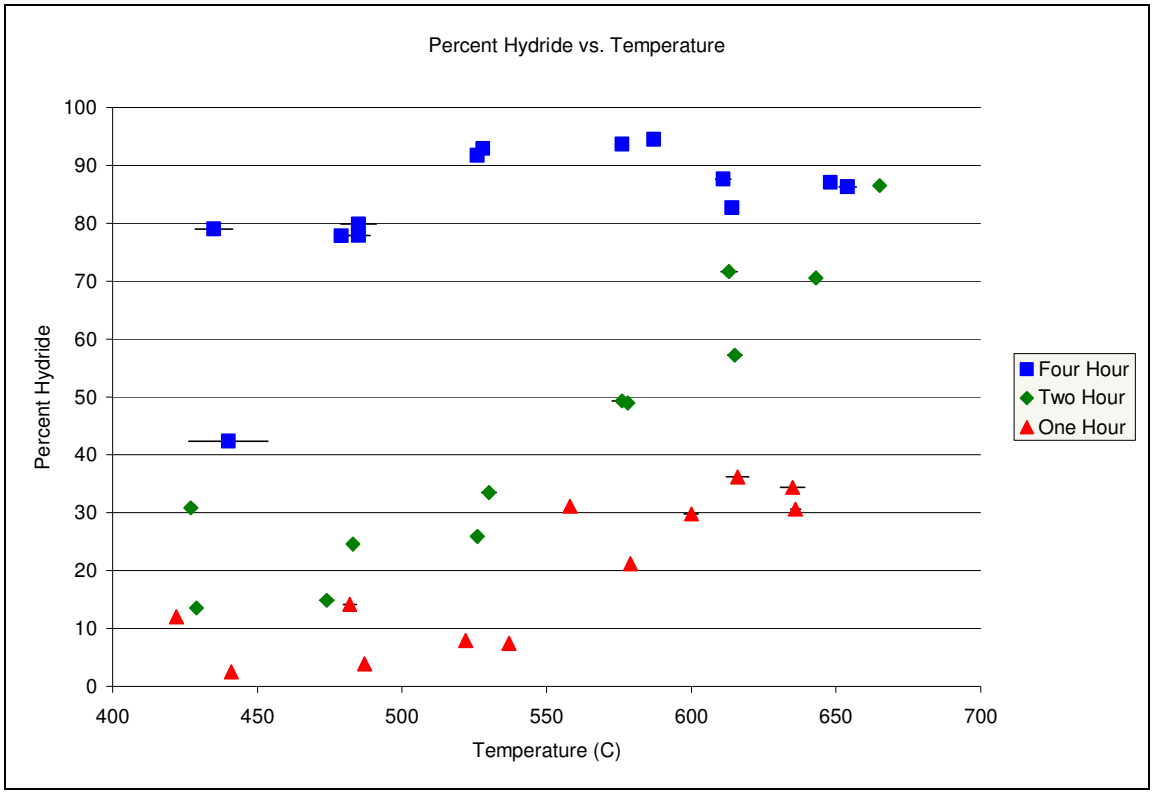

Figure 15. Formation of zirconium hydride as a function of temperature.

The results of this rate study were consistent with the expected behavior of hydrogen formation in Zircaloy-4. It can be seen from Figure 15 that the data displays a general trend of increasing P_H with increasing temperature, which is expected from a

thermally-activated process. It can also be seen that P_H is greater for longer reaction times, as would be expected

5. DISCUSSION OF EXPERIMENTAL RESULTS

In the previous section, results were presented for 87 experiments completed to evaluate hydride formation in Zircaloy-4 tubes; the final 44 of these experiments were completed to quantify the rate of hydride formation. This rate study was intended to be composed of 36 data points, but 7 experiments were repeated for various reasons. These reasons included pressure fluctuations, improper analysis, and obvious disagreement with expected trends.

5.1 Experimental Observations

The experiments performed prior to the rate study (Nos. 15 to 57) were focused on establishing methods and procedures to generate reliable data. These tests were plagued by nitrogen contamination which was eventually minimized by replacing a leaking relief valve, creating better seals on the gas supply, and most importantly, installing a nitrogen getter. Contamination from nitrogen (in air) is believed to cause an under prediction in the achievable P_H for a given time and temperature. While nitrogen causes a false indicated hydrogen pickup of 14 times the measured value by mass, it is also likely that nitrogen absorbed on the surface of the specimen greatly decreases the diffusion rate of hydrogen within the cladding. This effect is believed to be so limiting that it negates the over prediction caused by the difference in atomic masses resulting in an under prediction of P_H. This diffusion limiting characteristic is due to the fact that nitrogen occupies the octahedral positions, putting strain on the crystal lattice. [7] This has the effect of limiting the diffusion of hydrogen because the lattice strain makes it

energetically unfavorable for hydrogen atoms to occupy the tetrahedral sites in the immediate vicinity of any dissolved nitrogen atoms.

This effect should, at least in theory, hold true for oxygen contamination as well for the same reasons stated above. This was observable in the rate study tests because it was found to be difficult to acquire reproducibility for low temperatures and short hydride times. The data generated from the one hour tests generally had more scatter than the data from longer experiments. It is reasonable and consistent to speculate that this is related to the zirconium oxide surface layer present on all samples. This effect should be of concern if this process is to be used on an industrial scale, especially when considering spent fuel cladding. Spent fuel cladding is of special concern because it contains a thick outer oxide layer as well as an inner crud layer both of which were nonexistent for these experiments. These two features may be the Achilles heel of this process if it is to be used on an industrial scale for spent fuel cladding. A possible fix to this issue could be to remove as much of the crud layer as possible. The oxide layer can then be dissolved into the zirconium lattice by heat treatment at near 1100°C. This has been shown to greatly increase the hydride rate, especially for the initial stages of the hydride reaction. [7]

It was found that if this material is to be pulverized, it is much more desirable to produce zirconium hydride in the presence of alpha phase zirconium as opposed to beta phase zirconium. The α-Zr phase was seen to be dramatically more brittle after hydriding than the β-Zr phase, often disassembling itself into course, jagged particles during the reaction process. This is believed to be because the α-Zr solubility for

hydrogen is far lower than that of β-Zr, resulting in the earlier formation of significant quantities of the brittle δ-$ZrH_{1.6}$ phase. This transformation induces volumetric strains due to density changes associated with δ phase formation and the δ phase is fairly brittle. It can be seen from the phase diagram (Fig. 1) that at temperatures below the α-β-δ eutectoid temperature, the δ phase begins precipitating with very low hydrogen pickup. This is in contrast to temperatures above the eutectoid temperature in which delta phase does not begin to form until a P_H of 28% has been achieved. Another advantage to hydriding α-Zr is that the process may be completed at lower temperatures, which is important because nitrogen pickup is strongly temperature dependent and greatly increases at temperatures above 700°C. [7] A downside to the alpha phase pathway is that the hydrogen pickup rate is directly dependent on temperature. This means that it will take longer to produce materials with high hydrogen concentrations when operating in the alpha phase. However, for the sake of pulverization, this lower hydrogen pickup rate was seen to be insignificant. In fact, since hydriding α-Zr forms δ-$ZrH_{1.6}$ earlier in the process than when hydriding β-Zr, the low temperature process is more amenable to acceleration by *in situ* mechanical milling than the higher temperature scenario. It may therefore be possible to completely negate the rate limitations caused by low processing temperatures.

5.2 Hydride Formation Rate

Because it was observed that the reaction pathway of the hydride formation reaction has a strong impact on the brittleness of the material, it is desirable to develop a set of equations to predict hydrogen formation, and thus phase morphology, at any given

time. The data obtained in the rate study allows for the creation of a correlation which describes the time dependent behavior of hydride formation as a function of temperature. To this end, three possible formulations were explored. The first is the Avrami equation which is commonly applied to phase formation in metastable supersaturated solid solutions. The second was a parabolic rate law, which would be consistent with a diffusion-controlled process. The third was a simple linear fit of the data. There is no data-driven reason to select one of these fits over another, but the efficacy and applicability of each is discussed below.

A correlation was first formulated using the Avrami equation which is given by:

$$P_H = 1 - K * \exp(-t^n) \quad [6]$$

The hydride formation data from the rate study in Section 4 is plotted verses time in Figure 16 and the functional fit based on the Avrami form is also shown. The development of this correlation was accomplished by linearizing the Avrami equation such that it takes the form below.

$$\ln[-\ln(1 - P_H)] = \ln(K) + n \times \ln(t) \quad [7]$$

Where P_H is the time dependent fraction of completion of the hydride reaction, t is time, and both K and n are constants to be determined. The data was plotted using Equation 7, and a linear fit was created for each temperature series performed in the rate study. From these linear fits, the constants K and n in the Avrami equation were determined at each temperature, as summarized in Table 8 and Appendix B.

Table 8. Results of rate study using Avrami equation.

°C	K	n
440	0.047	2.077
480	0.104	2.099
520	0.073	2.506
560	0.334	1.437
600	0.424	1.126
640	0.471	1.181

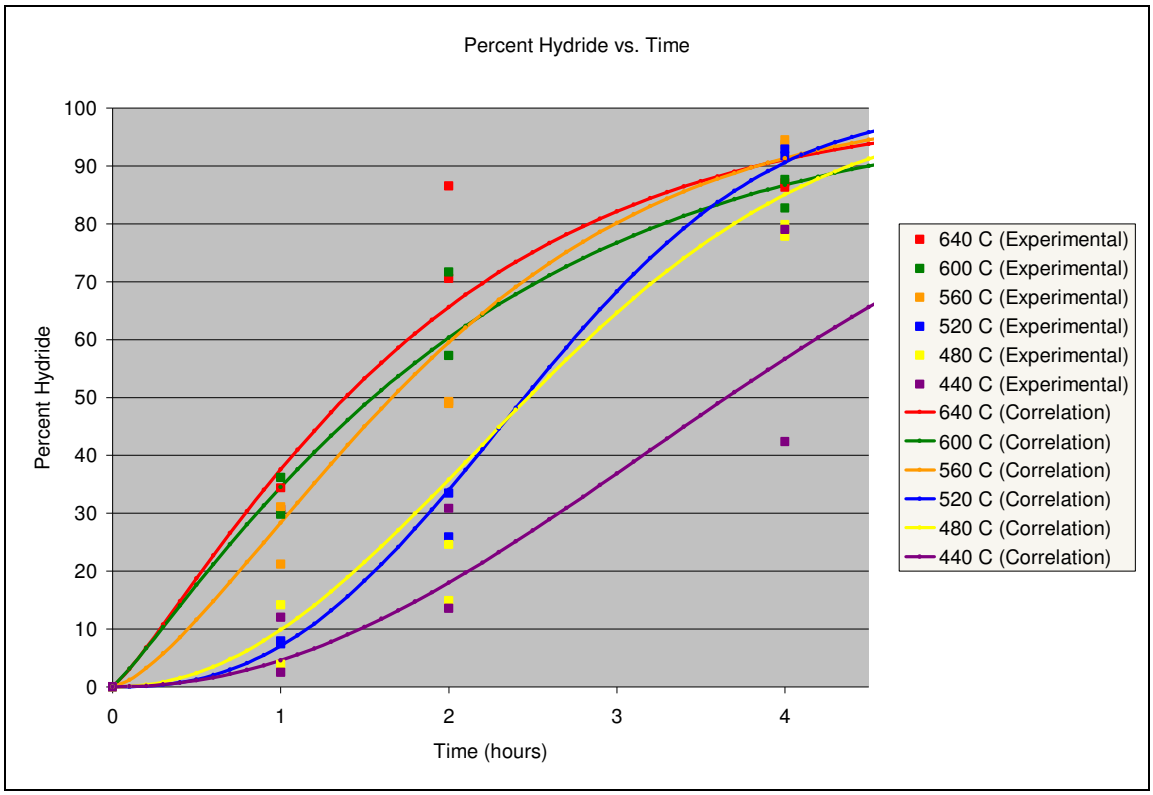

Figure 16. Time dependence of hydrogen pickup with Avrami correlation.

The fit from the Avrami equation is not satisfactory. This equation applies to chemical reactions and phase changes, which both apply to this series of experiments. However, it is also true that the equation is applicable for metastable phase transitions.

The experimental scenario provides hydrogen to the samples and it is expected that the hydrogen formation reaction proceeds at a rapid rate. Therefore, the hydride formation rate is limited by the transport of hydrogen from the process gas into the zirconium material and the Avrami supersaturation condition is never achieved. This correlation was therefore rejected but the above discussion is included here for completeness.

Because the hydride reaction is transport controlled, a parabolic formulation consistent with hydrogen diffusion in zirconium was considered next. [6] The parabolic correlation has the form given by Equation 1, shown below:

$$P_H = At^m \qquad [1]$$

Where P_H is the degree of completion of the reaction in percent ZrH_2, t is the time in hours, and A and m are constants to be determined. The data was plotted as a function of time for each temperature of interest and these constants were found by linearizing Equation 1 resulting in Equation 8.

$$\ln P_H = \ln A + m \ln t \qquad [8]$$

It was observed that for times of four hours and for temperatures of 600 ºC and 640ºC, the material had apparently already achieved saturation, so the curve fit was produced using only the data generated at one and two hours. The constants are tabulated in Table 9 and shown in Appendix C, and the experimental data is re-plotted with the parabolic correlation in Figure 17.

Table 9. Constants for parabolic hydride rate.

℃	A	m
440	5.7	1.70
480	6.8	1.72
520	7.9	1.80
560	26	0.94
600	33	0.96
640	32	1.27

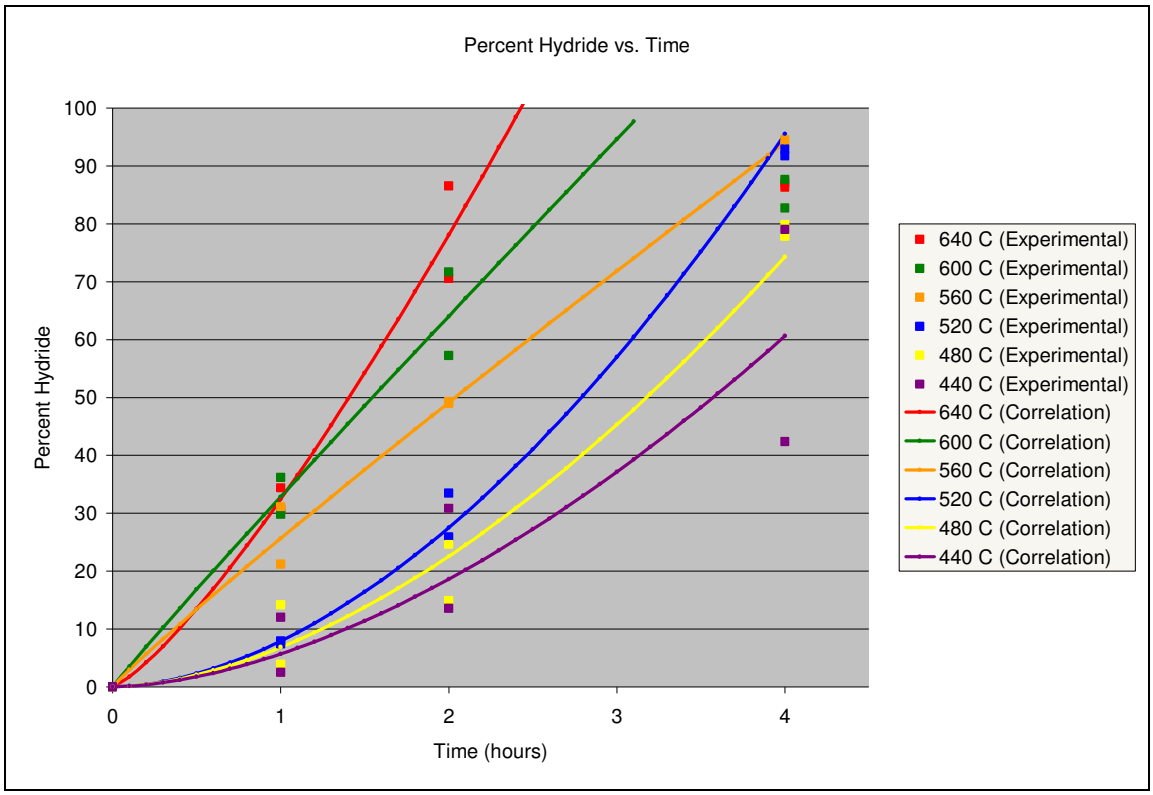

Figure 17. Time dependence of hydrogen pickup with parabolic correlation.

The data in Table 9 can then be used to predict the completion of the hydride reaction. It can also be useful to solve Equation 1 for the reaction time so that one may determine the length of time the hydride reaction should progress in order to achieve the

desired hydrogen content. Equations were developed for the constants A and m and are plotted in Figures 18-19 and shown in Equations 1 and 9.

$$\text{For } 440^{\circ}\text{C} < T < 540^{\circ}C$$
$$P_H = At^m$$
$$A = 0.028T - 6.39$$
$$m = 1.74 \pm 0.05 \qquad [1]$$

$$\text{For } 540^{\circ}C < T < 640^{\circ}C$$
$$P_H = At^m$$
$$A = 0.085T - 20.5$$
$$\text{m} = 1.1 \pm 0.2 \qquad [9]$$

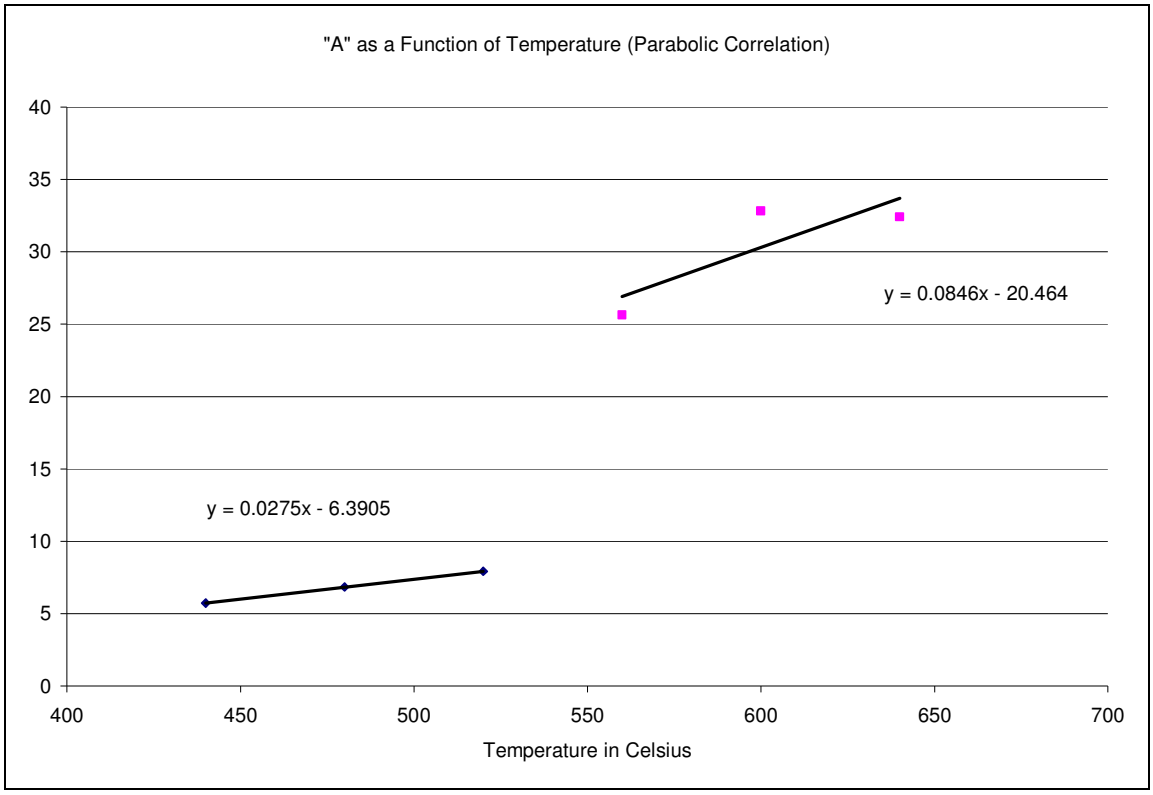

Figure 18. Plot showing step change in *A* at 540°C phase transition.

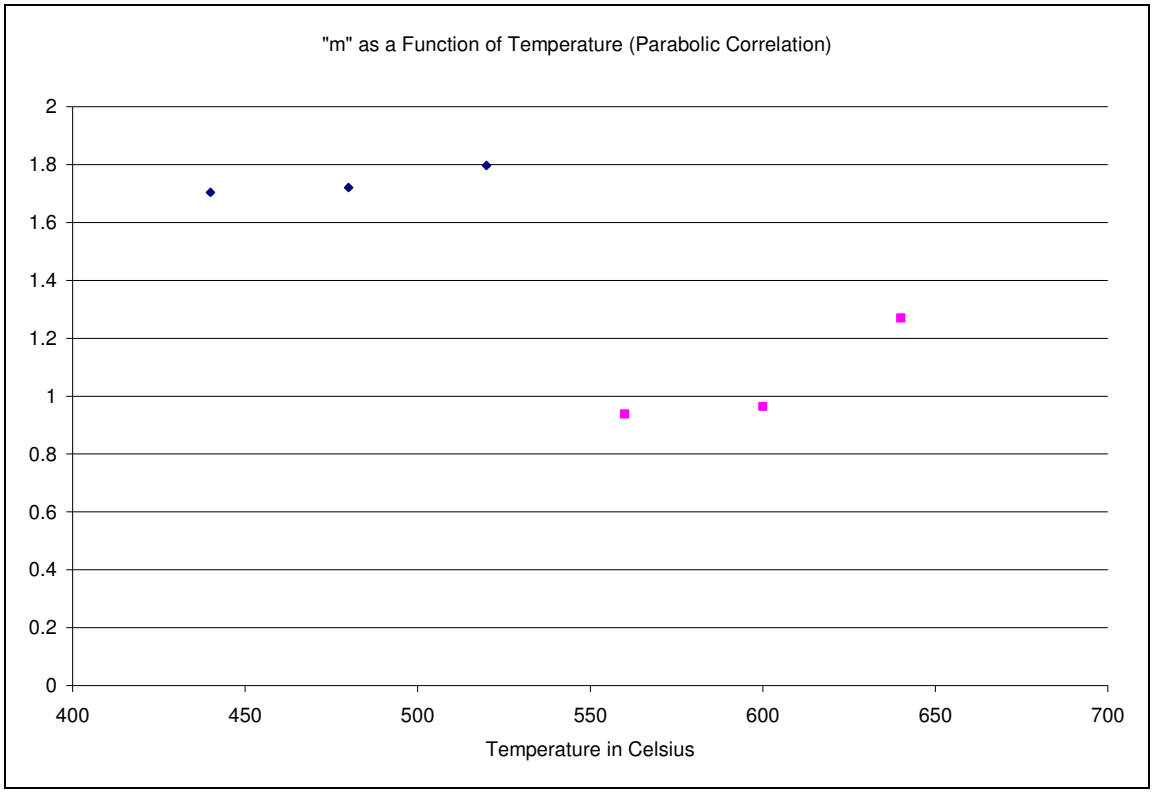

Figure 19. Plot showing step change in m at 540°C phase transition.

The correlation produced from the rate study is applicable at temperatures from 440°C to 640°C and times between one and four hours. Care should be taken if it is to be extrapolated to times less than one hour and for temperatures lower than 440°C due to issues regarding diffusion through the oxide layer as stated previously. This phenomenon is believed to be as important as the diffusion of hydrogen through the bulk of the material for low hydrogen concentrations. This correlation should be grossly predictive for times longer than four hours and for higher temperatures up until the samples reach P_H values approaching the saturation level, which occurs quite rapidly, but this extrapolation has not been demonstrated. It can be seen from the correlation that the

constants *A* and *m* exhibit a step change at the alpha beta phase transition. This step change is consistent with the α-Zr to β-Zr phase change.

This parabolic fit represents the data reasonably well, but it still has limitations as a physical representation of the hydride formation process. A textbook-style parabolic rate law for diffusion-controlled reaction (e.g., case hardening of steel) would have an exponent of m=0.5 and represent the diffusion of hydrogen through a surface reaction zone to measurable penetration depth before the formation reaction would occur. In the current experiments, the Zircaloy material crumbles under hydrogen exposure, typically within the first hour of the test, thus rapidly changing the amount of exposed surface area. Therefore, it is not a surprise that the m-values are not equal to 0.5. On the other hand, the calculated values of m (1.7±0.1 for α-Zr and 1.1±0.2 for β-Zr) indicate that a linear fit may be just as appropriate for the data.

A linear fit was produced (Appendix D) by fitting a line to the data for one and two hours as well as the point corresponding to a time and P_H equal to zero for each temperature. This linear fit agrees well with the data for the β-Zr phase, as would be expected based on the results from the parabolic correlation. However, the data obtained for the α-Zr phase seems to better fit the parabolic correlation. The parabolic fit with an "m" value greater than one implies that the reaction rate increases as a function of time for the α-Zr phase. This makes sense physically due to the time dependence of the material's surface area caused by the samples fracturing during the reaction. The data can be seen plotted with these two functional forms in Figure 20.

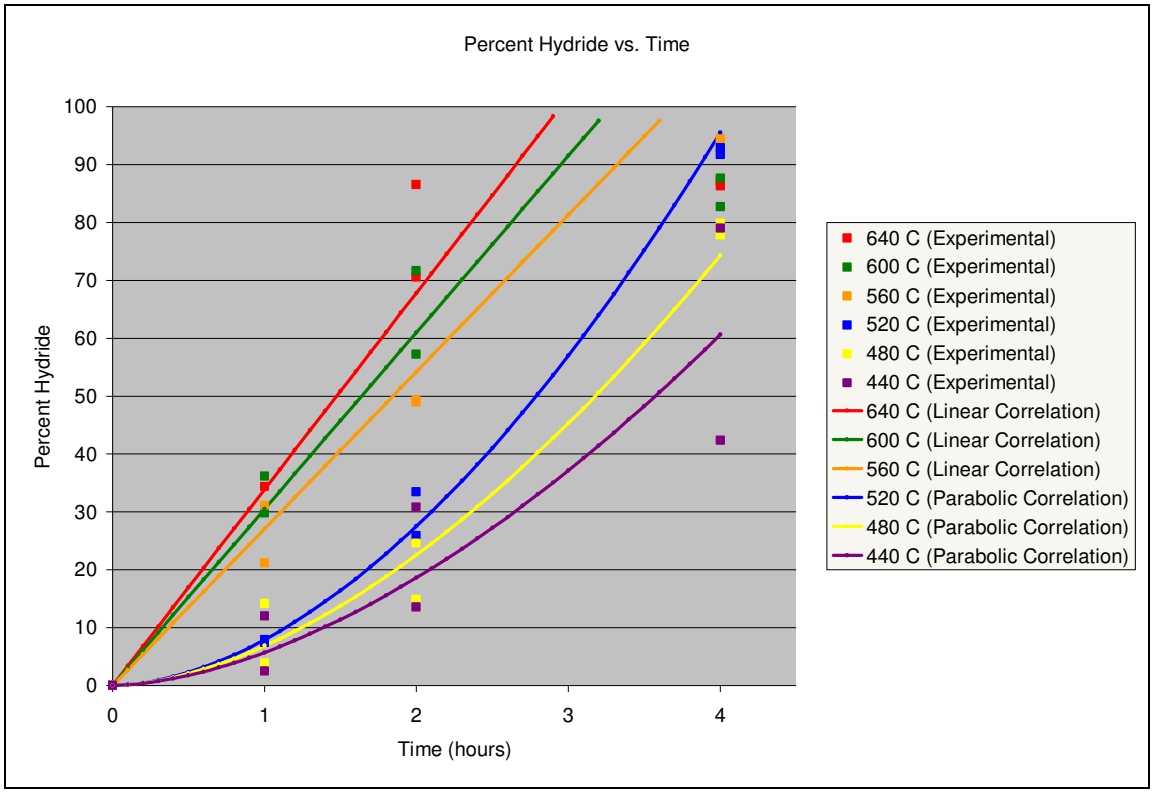

Figure 20. Data plotted with final correlation.

5.3 Apparent Activation Energy for Hydride Formation

An apparent activation energy of hydride formation in Zircaloy can be estimated using the calculated results from the previous section. This can be performed by assuming that the rate of change in P_H is a thermally activated phenomenon following an Arrhenius-style behavior, as represented by Equation 10. By linearizing this equation as shown in Equation 11, the apparent activation energy may be estimated.

$$R = R_o e^{-Q/kT}$$

$$\text{"R" is the reaction rate or } \frac{dP_H}{dt} \qquad [10]$$
"Q" is the activation energy
"k" is the gas constant
"T" is the temperature in $^{\circ}C$

$$\ln R = \ln R_o - Q/kT \qquad [11]$$

The Avrami correlation has been excluded from the activation energy analysis because there was not a physical basis for its use, nor did it accurately fit the data. It was determined from the preceding discussion that P_H along the β-Zr pathway expressed a linear relationship with respect to time, and P_H along the α-Zr pathway displayed a parabolic relationship. For the sake of this analysis, the reaction rates for the parabolic correlation were determined at a time equal to two hours. This is because at times near and below one hour, the data obtained was not as reliable. It was also apparent from the data that the samples often would reach saturation before four hours had expired, therefore two hours was chosen as the time for the sake of determining the activation energy. The activation energy obtained from the linear correlation for the β-Zr pathway was found to be 40 ±4 kJ/mol which roughly agrees with tabulated values of hydrogen diffusion in zirconium: 42 kJ/mol and 65.5 kJ/mol. [11] The activation energy for the α-Zr pathway was determined using the parabolic correlation, and was found to be 26 ±3 kJ/mol. This lower activation energy is believed to be due to the samples disassembling themselves during the reaction, which increases the surface area of the material, and would express itself as a decrease in activation energy. This time dependence of the

surface area makes it extremely difficult to obtain activation energies which are consistent with hydrogen diffusion in zirconium.

It should be noted that the activation energies produced from these correlations are not true activation energies, but rather apparent activation energies which are specific to this process. It was difficult to get true activation energies for diffusion of hydrogen in α-Zr because the samples had the tendency to disassemble during the reaction. If true diffusion activation energies are to be obtained, the change in surface area with respect to time needs to be taken into account.

6. SUMMARY AND RECOMMENDATIONS

Small tube samples of nuclear grade Zircaloy-4 were exposed to flowing argon-5% hydrogen to quantify the first step in a processing concept proposed for the recycle of spent nuclear fuel cladding. The procedures developed by this research and the resulting data can be used to efficiently produce a zirconium hydride powder. The proposed Zircaloy recycle process will hydride and mill Zircaloy cladding tubes to produce fine hydride powder and then dehydride the powder to produce metal; the research described above is exclusively focused on understanding the hydride formation reaction.

The principal outcomes and observations from this work may be summarized as follows:

1. The hydride formation experimental system was perfected and the procedures described in Section 3.2 were used to perform a systematic study of the reaction vs. time and temperature.
2. One of the most significant obstacles to the generation of reliable data was nitrogen contamination in the process gas. Great efforts were made in the purification of the process gas by way of better seals and the addition of a high temperature titanium sponge nitrogen getter. These efforts were seen to dramatically increase the reproducibility and predictability of the data obtained.

3. Hydride formation was observed to proceed rapidly in the absence of nitrogen contamination in the gas. For temperature ranging from 480°C to 640°C, the reaction was typically complete in less than 4 hours.
4. It was observed that the P_H measurements were easier to reproduce at higher temperatures and when the reaction was allowed to proceed for longer periods of time. This is believed to be caused by the oxide boundary layer inhibiting hydrogen diffusion.
5. It was observed that for temperatures above the α-β-δ eutectoid the samples maintained a relative toughness. It was also found that at temperatures below this eutectoid the samples readily ground to a powder, and often times would disassemble during the reaction process resulting in small shards of zirconium hydride. This is believed to be due to the precipitation of the brittle δ-Zr phase at low hydrogen concentrations along the α-Zr phase pathway.
6. A correlation was produced for a temperature range of 440-640°C and hydride times of 1-4 hours. It was found that for temperatures above the α-β-δ eutectoid the P_H data were well represented by a linear dependence with respect to time, while for temperatures below this eutectoid the P_H data were well represented by a parabolic trend with respect to time. The equations are given below.

$$\begin{aligned} &\text{For } 440^{\circ}\text{C} < T < 540^{\circ}C \\ &P_H = At^m \\ &A = 0.028T - 6.39 \\ &m = 1.74 \pm 0.05 \end{aligned} \qquad [1]$$

For $540^{\circ}\mathrm{C} < T < 640^{\circ} C$

$$P_H = At \qquad [2]$$

$$A = 0.085T - 20.5$$

7. Apparent activation energy was extracted from these correlations. For the parabolic correlation the activation energy was found by calculating the rate of hydride formation from the slope of the function at a time equal to two hours, while the rate of hydride formation is simply equal to the value of *A* for the linear correlation. The activation energies for these respective correlations were found from the Arrhenius equation shown below. The apparent activation energy for the β-Zr pathway was found to be 40 ± 4 kJ/mol, and 26 ± 3 kJ/mol for the α-Zr pathway.

$$R = R_o e^{-Q/kT} \qquad [10]$$

The following observations and recommendations are presented to assist further research in this area.

1. It is strongly recommended that any nitrogen contamination from the air be removed by thoroughly sealing the system and by the addition of a nitrogen getter device.
2. This research proved that the hydride method can be used to produce a zirconium hydride powder. However, the hydride reaction by itself is not sufficient to producing a powder on its own and subsequent milling or grinding must be performed.

3. A systematic study of the reaction kinetics is recommended to gain understanding into the apparent activation energy. The activation energies presented in this thesis are merely apparent activation energies based on the measured results. While hydride formation in zirconium is known to be diffusion controlled, it becomes difficult to quantify this effect on Zircaloy-4 tubes. This is due to the presence of an oxide passivation layer, as well as an observed increase in surface area resulting from the material disassembling itself during the hydride reaction.
4. *In situ* observation of the reaction progress could be monitored using hot stage crystallography to better understand the effect of precipitation of the brittle δ-phase.

REFERENCES

[1] S.M. McDeavitt, A. Parkison, A.R. Totemeier and J.J. Wegener, Fabrication of Cermet Nuclear Fuels Designed for the Transmutation of Transuranic Isotopes, Materials Science Forum, 561-565: 1733-1736 (2007).

[2] J.C. Haygarth and R.A. Graham, Oremet-Wah Chang Presentation to Argonne National Laboratory, private communication.

[3] D.T. Kraemer, (2005). Establishing Methods for Recycling Spent Zircaloy Cladding Using a Hydride-Dehydride Processing Route. M.S. Thesis, Purdue University, West Lafayette, IN.

[4] S.M. McDeavitt, (1992). Hot Isostatic Pressing of U-10Zr Alloy Nuclear Fuel by Coupled Grain Boundary Diffusion and Power-Law Creep. Ph. D. Dissertation, Purdue University, West Lafayette, IN.

[5] J.J. McKetta and G.E. Weismantel eds., Encyclopedia of Chemical Processing and Design, v. 58, Thorium and Thorium Compounds Supply-Demand Relationships, Marcel Dekker, Inc. New York, 1997 pp.78-85.

[6] B. Lustman and F. Kerze Jr., The Metallurgy of Zirconium, McGraw-Hill Book Company, Inc, New York, 1955.

[7] G.L. Miller, Metallurgy of the Rarer Metals-2: Zirconium, 2nd edition, Academic Press Inc., Publishers, New York, 1957.

[8] R.A. Hard and J.A. Megy, (1984). U.S. Patent No. 4,470,847. Washington DC: U.S. Patent and Trademark Office.

[9] H. S. Kalish, The Preparation of Zirconium Powder. Zirconium and Zirconium Alloys, American Society for Metals (1953): 5-36.

[10] W.M. Mueller, J.P Blackledge, and G.G. Libowitz, Metal Hydrides, Academic Press, New York, 1968.

[11] Y.R. Rashid, D.J. Sunderland, and R.O. Montgomery, Creep as the Limiting Mechanism for Spent Fuel Dry Storage, EPRI, Palo Alto, CA: 2000. 1001207.

APPENDIX A

RAW DATA FROM HYDRIDE EXPERIMENTS

Experiment number	% Hydrogen used	Flow rate at end of experiment (SCFH)	Pressure (" H20)	Temperature (degrees Celsius)	Time (hrs)	sample mass (g)	actual % if all hydride	mass increase (g)
1	4.83	8	28	360	6	2.3805	#VALUE!	?
2	4.83	3	12	733	6	3.5256	69.79771	0.0534
3	4.83	7	25	518	6	4.1906	74.33673	0.0676
4	4.83	3.5	4.5	477	12	3.6519	14.13293	0.0112
5	4.83	7	24	503	12	3.7222	91.49085	0.0739
6	4.83	3	12	522	23.5	3.7565	99.24259	0.0809
7	5.02	7.75	25.5	525	24	3.281	98.87793	0.0704
8	0	7.5	25	488	6	3.7812	3.046796	0.0025
9	5.02	6.5	23	603	6	3.7473	87.80368	0.0714
10	5.02	8	26.5	543	8	4.0353	50.01857	0.0438
11	0	7.5	22	546	12.5	3.657	2.520217	0.002
12	5.02	7.5	25.5	755	5.2	3.1764	44.68363	0.0308
13	4.97	7.4	23	529	12	8.1227	11.97057	0.0211
14	4.97	7.5	24	539	8	3.2039	70.62126	0.0491
15	4.97	5	10.75	521	6	2.676	17.90936	0.0104
16	4.97	5	10.75	517	6	2.7359	11.28516	0.0067
17	4.97	5	24.75	534	6.3	2.8495	91.69536	0.0567
18	4.97	5	24.75	529	6.3	2.9652	65.2722	0.042
19	4.97	5	10.25	518	6	3.1677	11.05611	0.0076
20	4.97	5	24.25	353	6	3.5114	5.643144	0.0043
21	5.1	5	23.25	451	6	3.5418	6.245255	0.0048
22	5.1	5	25	541	6	3.5194	5.368441	0.0041
23	5.1	5	25	647	6	3.5042	15.25464	0.0116
24	5.1	5	25	747	7	3.5464	48.33794	0.0372
25	5.1	5	25	344	12	3.5213	0.785202	0.0006
26	4.97	5	25	547	6	3.5291	84.8755	0.065
27	5.1	5	25	543	6	3.5555	58.9717	0.0455
28	4.97	5	23.5	543	6	3.5118	43.8278	0.0334
29	4.97	4.5	27	542	6	3.5481	24.15739	0.0186
30	4.97	5	23.25	544	24	3.4936	61.20371	0.0464
31	4.97	4.75	25.5	519	24	3.5085	107.4397	0.0818
32	0	5	25	519	26	3.5395	4.296403	0.0033
33	5.1	5	25	517	24	3.5761	12.75729	0.0099
34	5.5	4.75	23.5	532	24	3.5226	20.27689	0.0155
35	5.5	4.8	25.5	501	24	3.5094	13.13107	0.01
36	5.5	5	25	522	24	3.482	24.35129	0.0184
37	5.1	5	25	510	24	3.5748	18.4339	0.0143
38	5.1	5	24.5	525	24	3.5143	47.33706	0.0361
39	5.1	5	25	572	21	3.486	36.22064	0.0274

Experiment number	% Hydrogen used	Flow rate at end of experiment (SCFH)	Pressure (" H20)	Temperature (degrees Celsius)	Time (hrs)	sample mass (g)	actual % if all hydride	mass increase (g)
40	4.94	5	25	582	24	3.566	89.6832	0.0694
41	4.94	5	25	556	24	3.532	96.80909	0.0742
42	4.94	5	25.5	570	6	3.5776	84.49772	0.0656
43	4.94	5	23.75	570	18	3.5606	96.93745	0.0749
44	4.94	4.5	22	563	12	3.4639	91.3954	0.0687
45	0	5	25	567	21	3.5054	5.915724	0.0045
46	4.94	5	24	310	24	3.5144	56.64551	0.0432
47	4.94	5	25.75	432	24	3.5994	85.90637	0.0671
48	5	5	24.5	572	6	3.56	71.5827	0.0553
49	5	5	25	566	6	3.5821	77.702	0.0604
50	5	5	25	566	6	3.5644	53.26522	0.0412
51	5	5	25	565	6	3.5419	17.30407	0.0133
52	5	1	25	571	6	3.5641	21.46304	0.0166
53	5	3	25	574	6	3.4982	90.2358	0.0685
54	5	3.2	26	575	6	3.5348	92.03919	0.0706
55	5	3	25	567	4	3.6144	34.67893	0.0272
56	5	3	25	576	4	3.6108	72.23471	0.0566
57	5	3	25	579	4	3.6114	45.6815	0.0358
58	5	3	25	568	4	3.6014	93.66399	0.0732
59	5	3	24	568	4	3.5544	94.51357	0.0729
60	5	3	25	519	4	3.5864	91.74289	0.0714
61	5	3	25	520	4	3.5254	92.93818	0.0711
62	5	3	25	481	4	3.6004	77.94701	0.0609
63	5	2.9	27	485	4	3.5205	79.84697	0.061
64	5	2.4	30	481	4	3.5453	93.97628	0.0723
65	5	3	25	569	1	3.5505	42.83092	0.033
66	5	3	25	579	1	3.6361	21.16477	0.0167
67	5	3	25	600	1	3.5888	29.79008	0.0232
68	5	2.9	30	479	4	3.5632	77.85549	0.0602
69	5	0.1	30	435	4	3.5464	79.00395	0.0608
70	5	3	25	436	1	3.4028	0.812546	0.0006
71	5	3	25	522	1	3.6209	7.890565	0.0062
72	5	3	25	440	4	3.5572	42.36161	0.0327
73	5	3	25	526	2	3.5905	25.92563	0.0202
74	5	3	25	422	1	3.5592	12.04103	0.0093
75	5	3	25	441	1	3.5388	2.474176	0.0019
76	5	3	25	436	2	3.5991	0.896266	0.0007
77	5	3	25	530	2	3.5389	33.46554	0.0257
78	5	3	25	611	4	3.5504	87.61116	0.0675
79	5	3	25	616	1	3.5507	36.20955	0.0279
80	5	3	25	614	4	3.5706	82.72748	0.0641

Experiment number	% Hydrogen used	Flow rate at end of experiment (SCFH)	Pressure (" H20)	Temperature (degrees Celsius)	Time (hrs)	sample mass (g)	actual % if all hydride	mass increase (g)
81	5	3	25	576	2	3.571	49.29541	0.0382
82	5	3	25	654	4	3.5448	86.31957	0.0664
83	5	3	25	648	4	3.5822	87.0907	0.0677
84	5	3	25	578	2	3.5553	48.99463	0.0378
85	5	3	25	665	2	3.5585	86.50524	0.0668
86	5	3	25	643	2	3.5459	70.56775	0.0543
87	5	3	25	613	2	3.5877	71.67225	0.0558
88	5	3	25	615	2	3.5675	57.22327	0.0443
89	5	3	25	537	1	3.5392	7.421688	0.0057
90	5	3	25	635	1	3.5684	34.35113	0.0266
91	5	3	25	487	1	3.5441	3.900751	0.003
92	5	3	25	636	1	3.6143	30.5999	0.024
93	5	3	25	477	2	3.543	61.52094	0.0473
94	5	3	25	475	2	3.5891	63.68381	0.0496
95	5	3	25	482	1	3.5756	14.17675	0.011
96	5	0	25	~440	?	3.5649	0.129266	0.0001
97	5	3	25	429	2	3.5674	13.56346	0.0105
98	5	3	25	558	1	3.6021	31.08733	0.0243
99	5	3	25	483	2	3.6343	24.5988	0.0194
100	5	3	25	427	2	3.5719	30.83412	0.0239
101	5	3	25	474	2	3.5672	14.85605	0.0115

APPENDIX B

CONSTANTS FROM AVRAMI CORRELATION

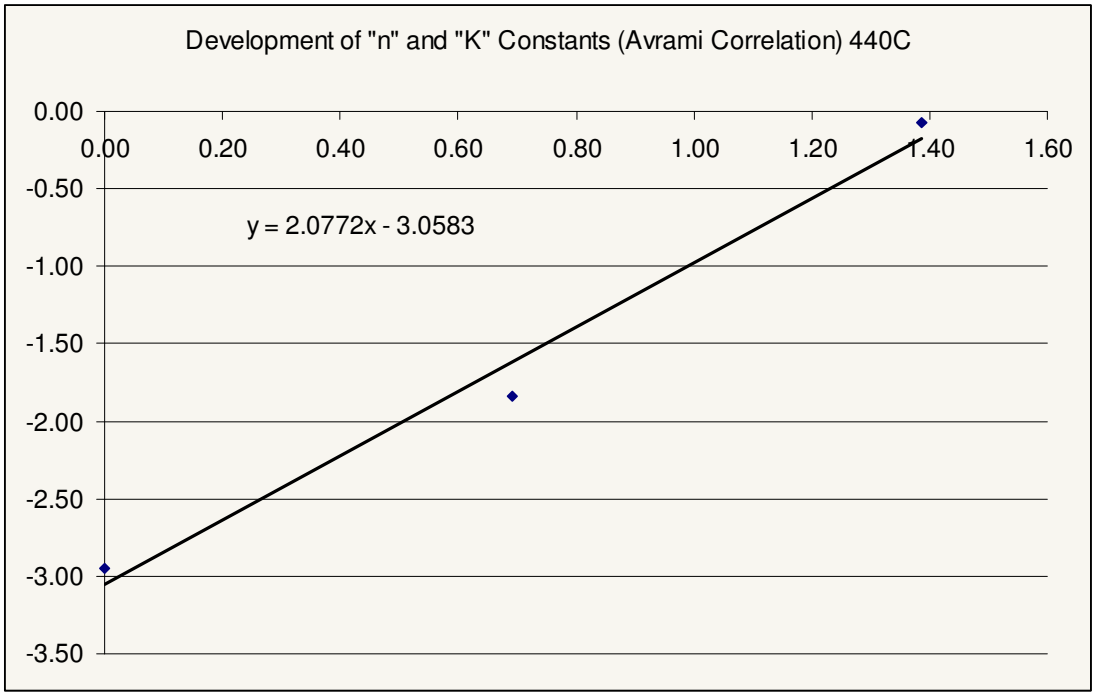

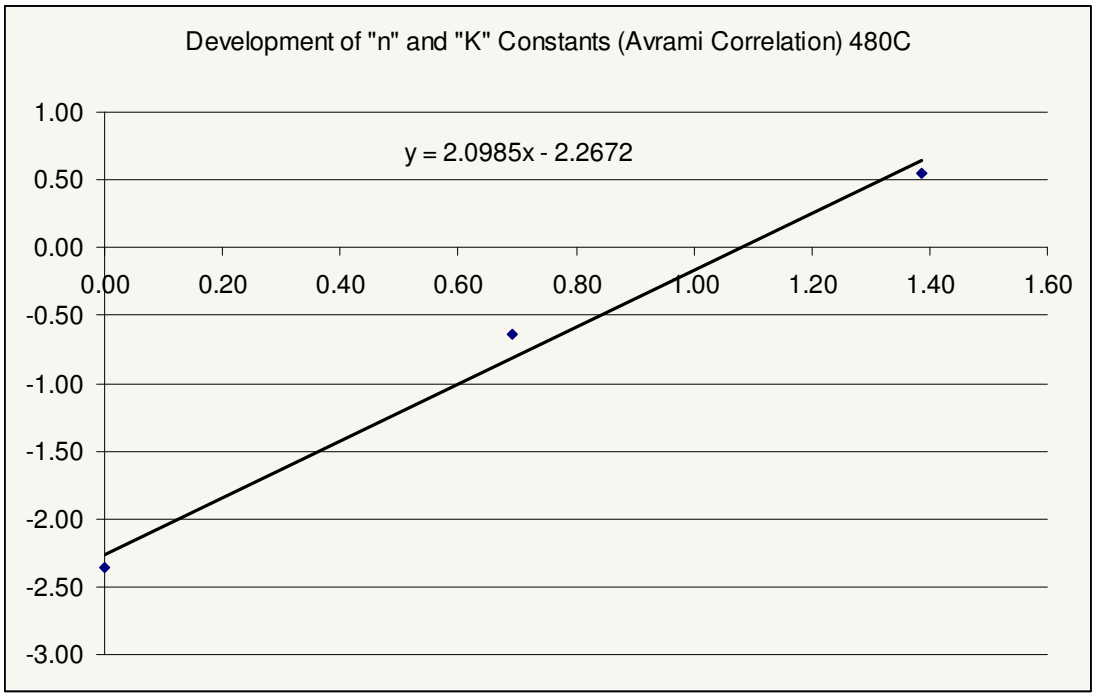

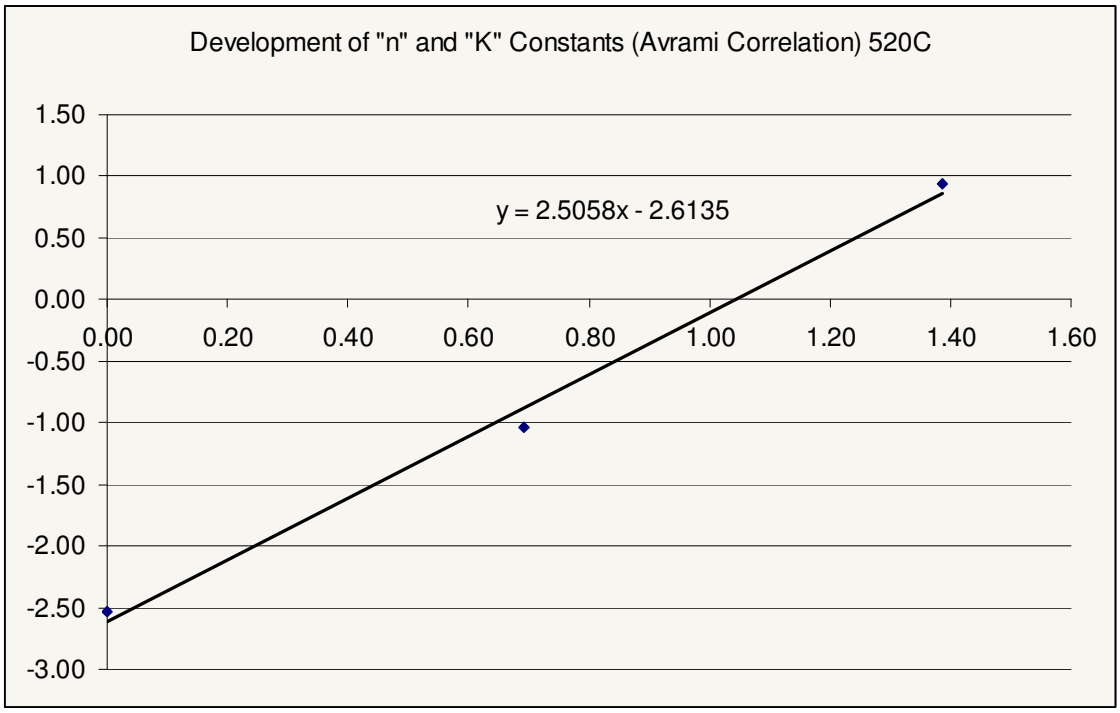
Development of "n" and "K" Constants (Avrami Correlation) 520C
y = 2.5058x - 2.6135
1.50
1.00
0.50
0.00
-0.50
-1.00
-1.50
-2.00
-2.50
-3.00
0.00
0.20
0.40
0.60
0.80
1.00
1.20
1.40
1.60

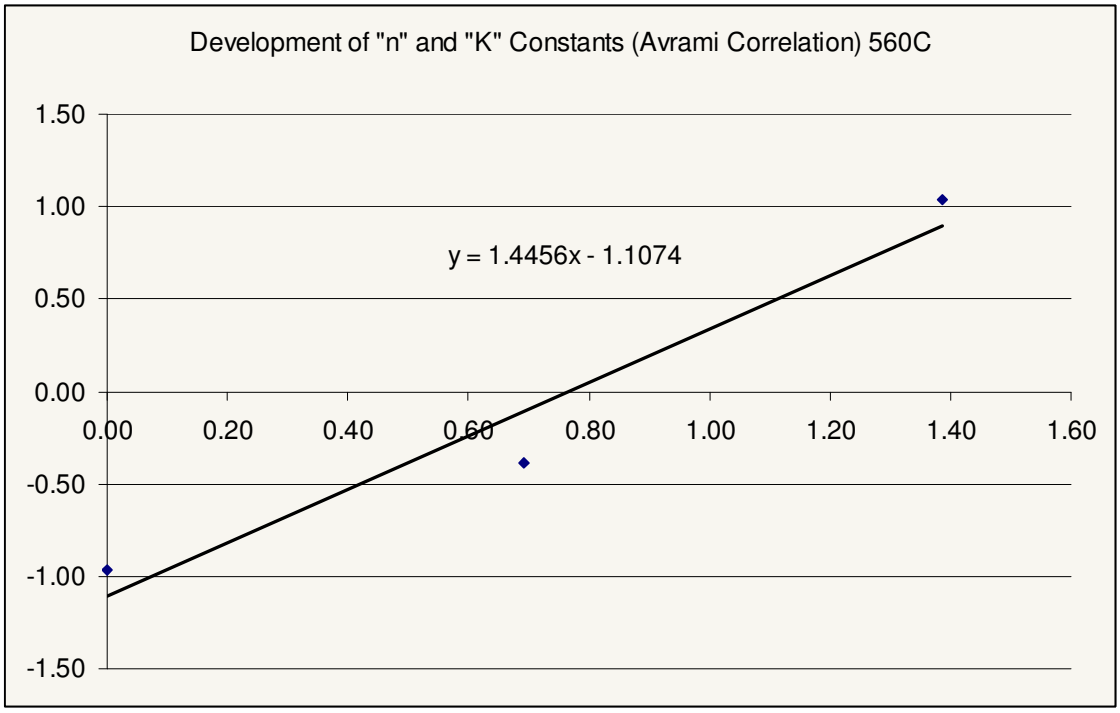
Development of "n" and "K" Constants (Avrami Correlation) 560C
y = 1.4456x - 1.1074
1.50
1.00
0.50
0.00
-0.50
-1.00
-1.50
0.00
0.20
0.40
0.60
0.80
1.00
1.20
1.40
1.60

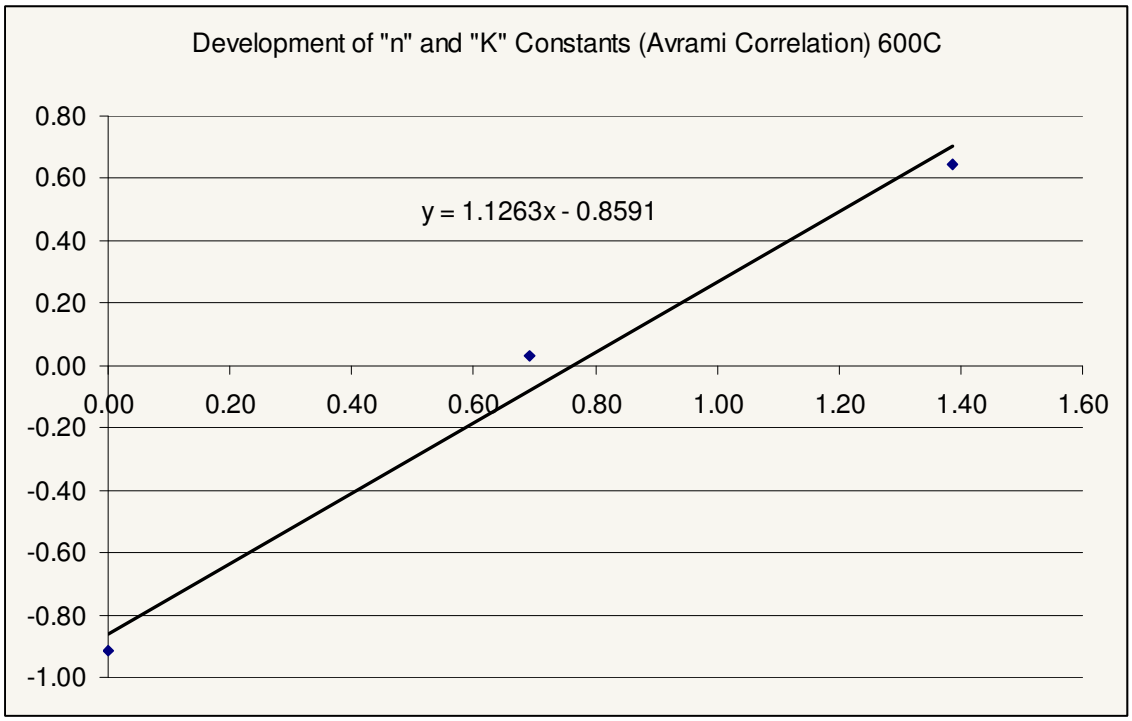
Development of "n" and "K" Constants (Avrami Correlation) 600C
y = 1.1263x - 0.8591
0.80
0.60
0.40
0.20
0.00
-0.20
-0.40
-0.60
-0.80
-1.00
0.00
0.20
0.40
0.60
0.80
1.00
1.20
1.40
1.60

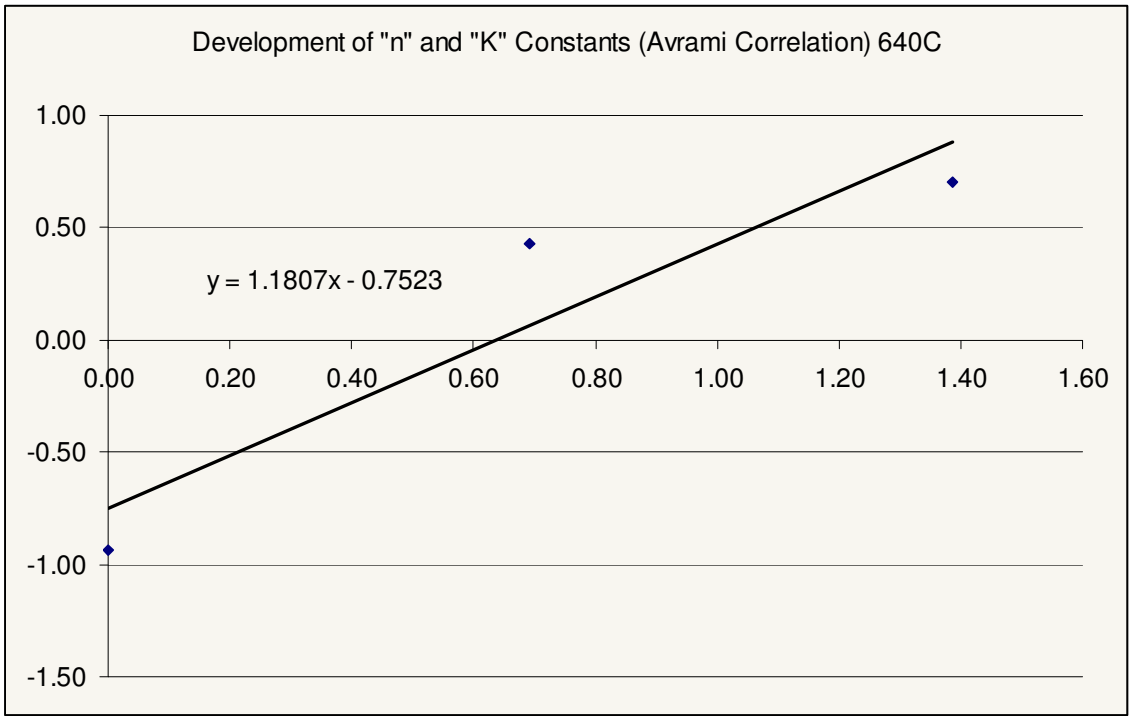
Development of "n" and "K" Constants (Avrami Correlation) 640C
y = 1.1807x - 0.7523
1.00
0.50
0.00
-0.50
-1.00
-1.50
0.00
0.20
0.40
0.60
0.80
1.00
1.20
1.40
1.60

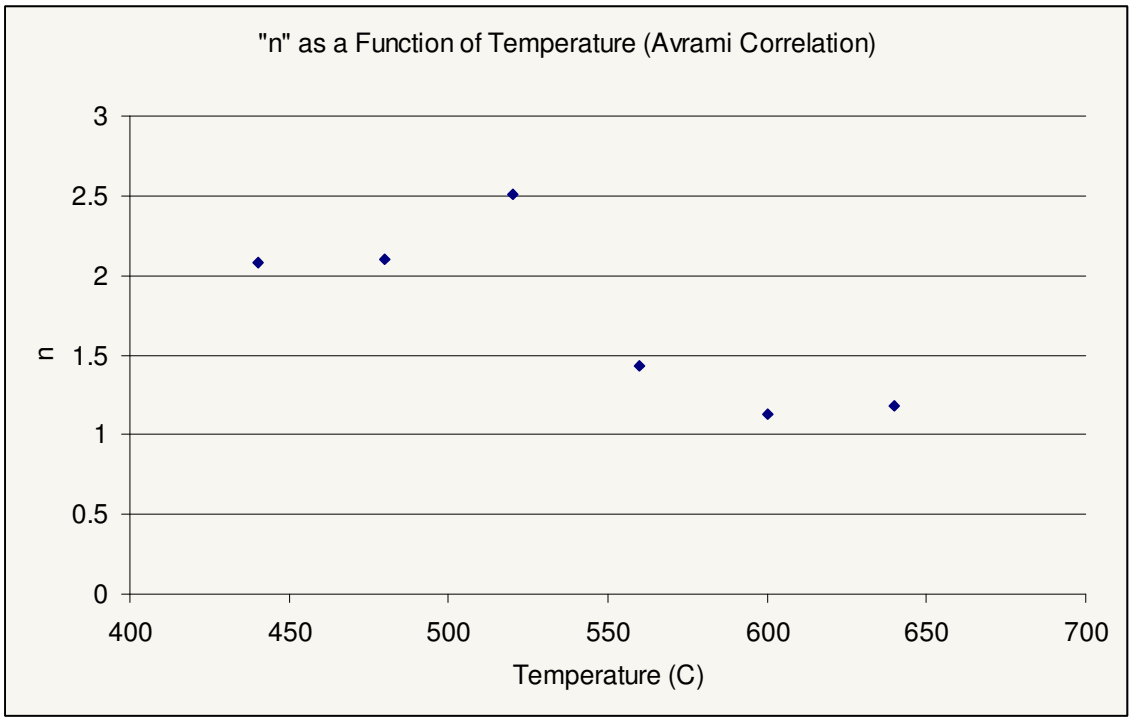
"n" as a Function of Temperature (Avrami Correlation)
n
3
2.5
2
1.5
1
0.5
0
400
450
500
550
600
650
700
Temperature (C)

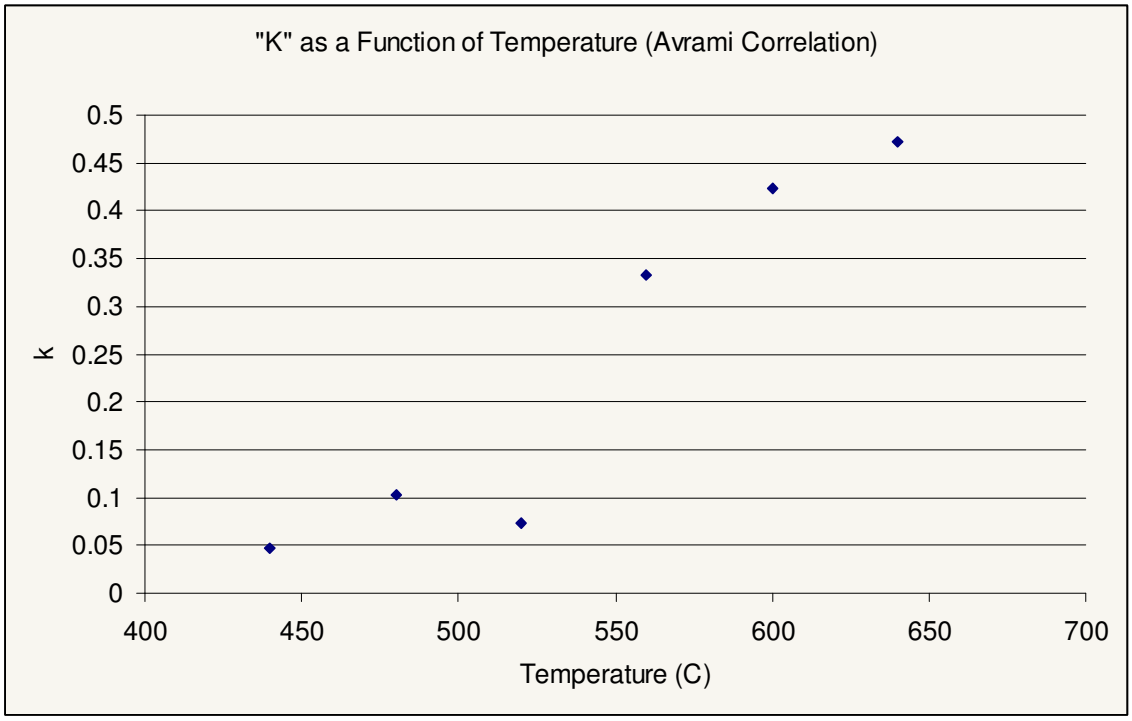
"K" as a Function of Temperature (Avrami Correlation)
k
0.5
0.45
0.4
0.35
0.3
0.25
0.2
0.15
0.1
0.05
0
400
450
500
550
600
650
700
Temperature (C)

APPENDIX C

CONSTANTS AND Q VALUE FROM PARABOLIC CORRELATION

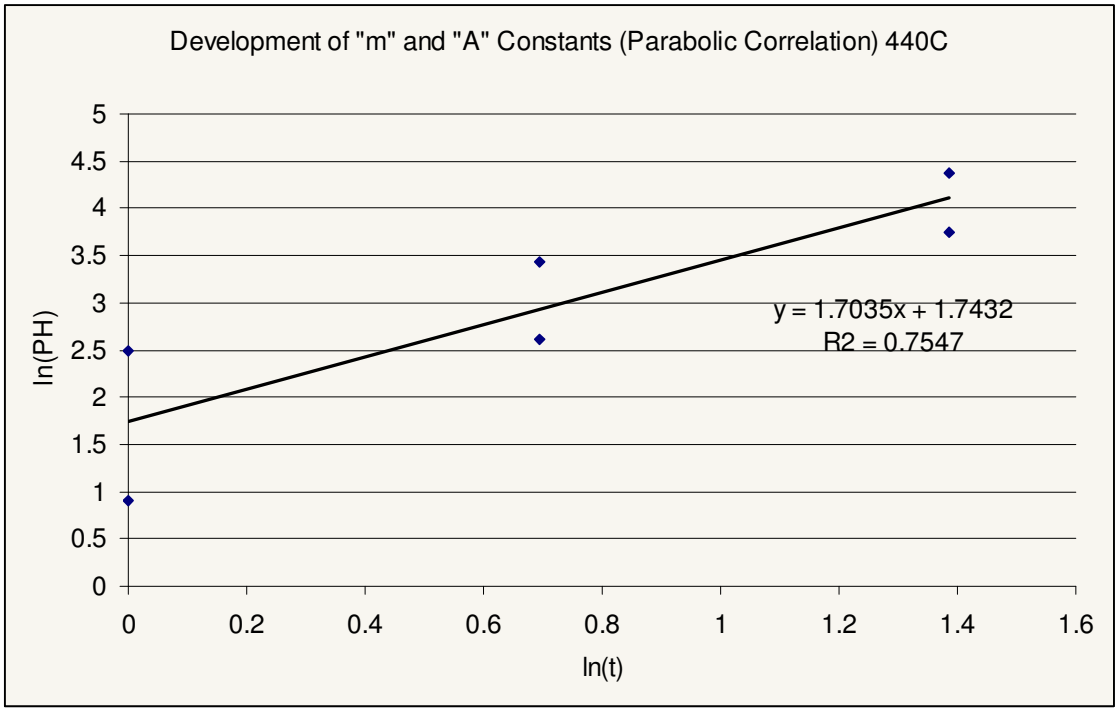

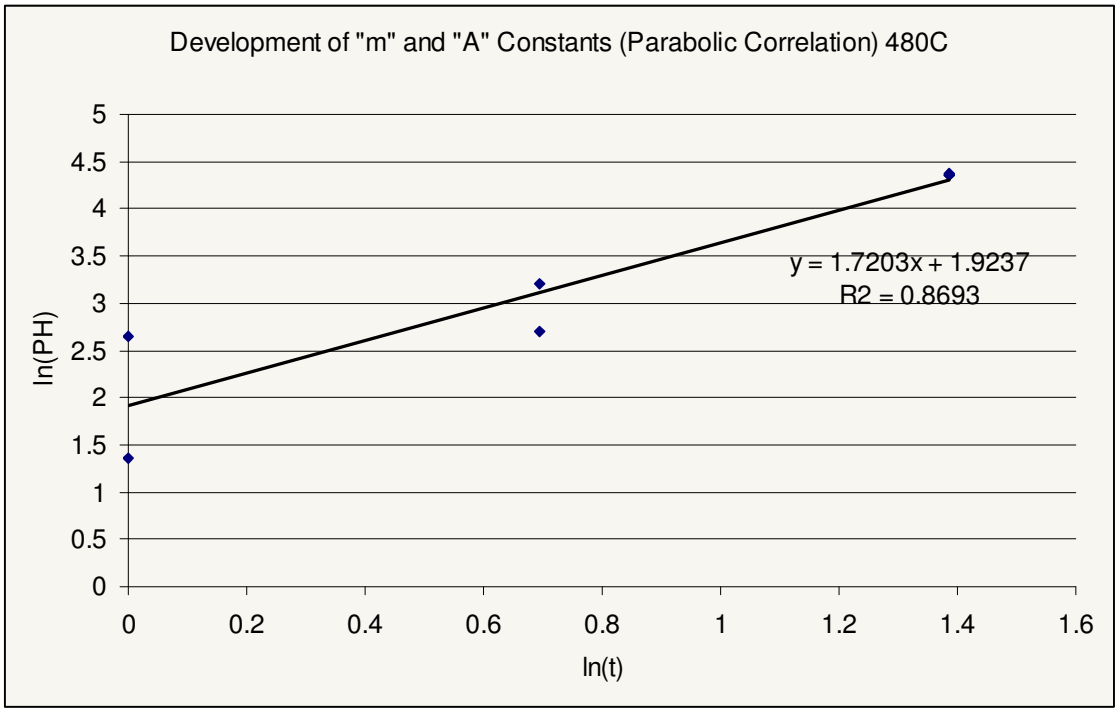

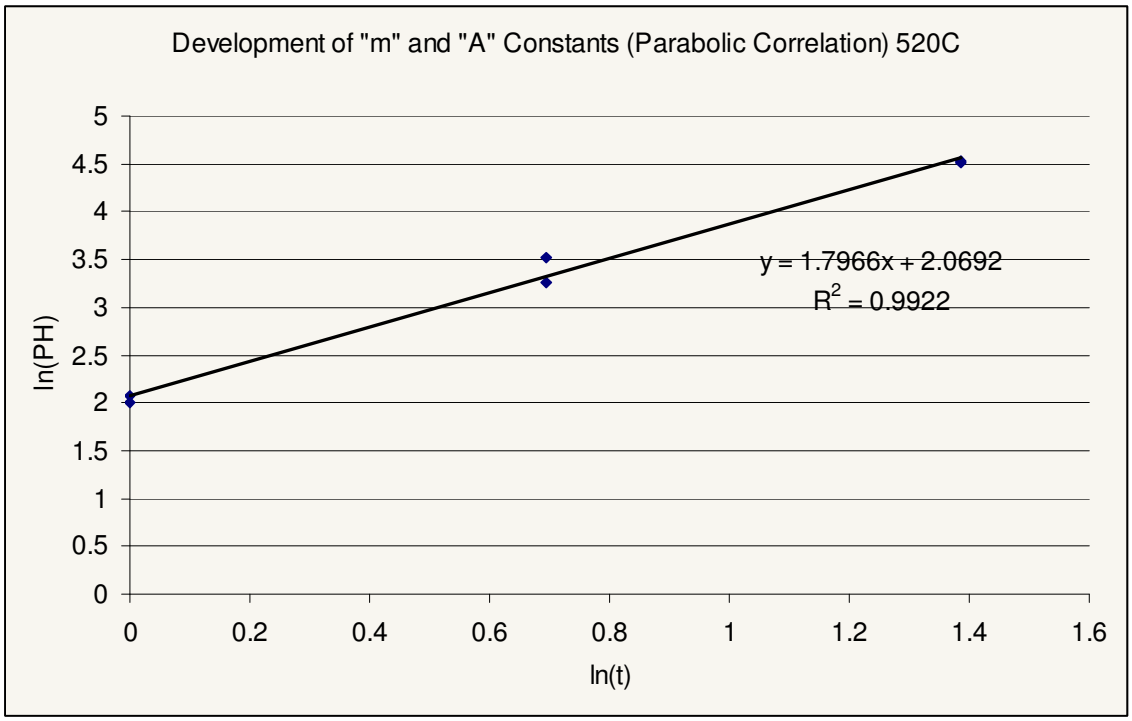
Development of "m" and "A" Constants (Parabolic Correlation) 520C
y = 1.7966x + 2.0692
R2 = 0.9922
ln(PH)
ln(t)
0
0.5
1
1.5
2
2.5
3
3.5
4
4.5
5
0
0.2
0.4
0.6
0.8
1
1.2
1.4
1.6

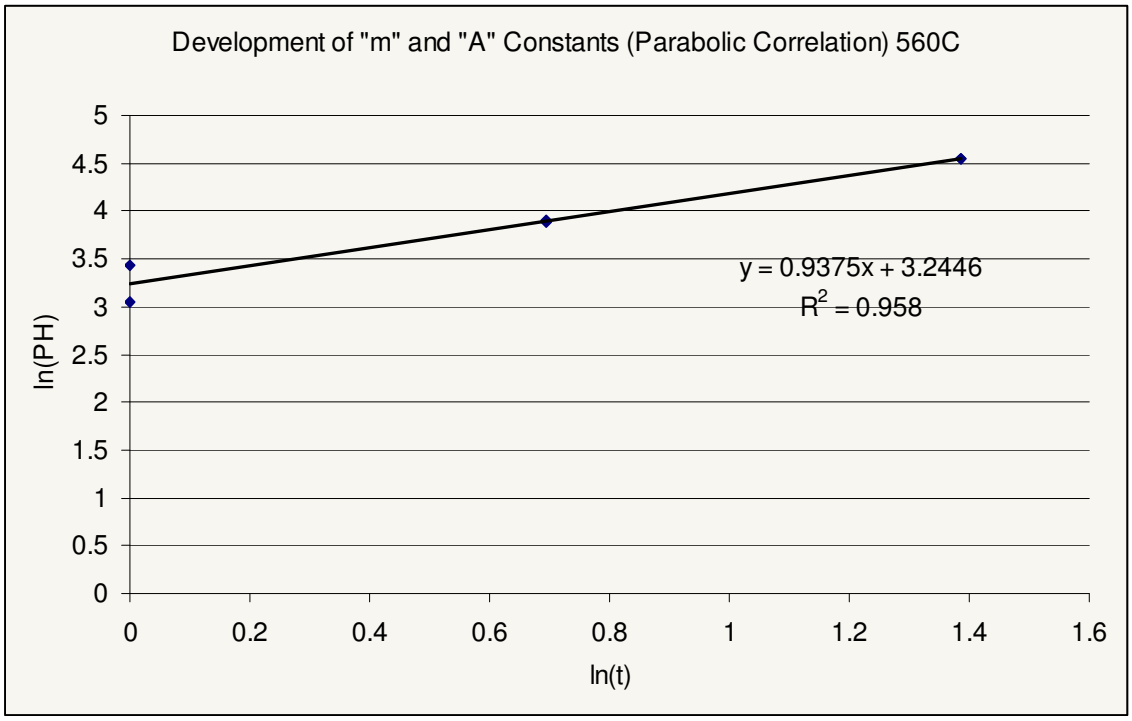
Development of "m" and "A" Constants (Parabolic Correlation) 560C
y = 0.9375x + 3.2446
R2 = 0.958
ln(PH)
ln(t)
0
0.5
1
1.5
2
2.5
3
3.5
4
4.5
5
0
0.2
0.4
0.6
0.8
1
1.2
1.4
1.6

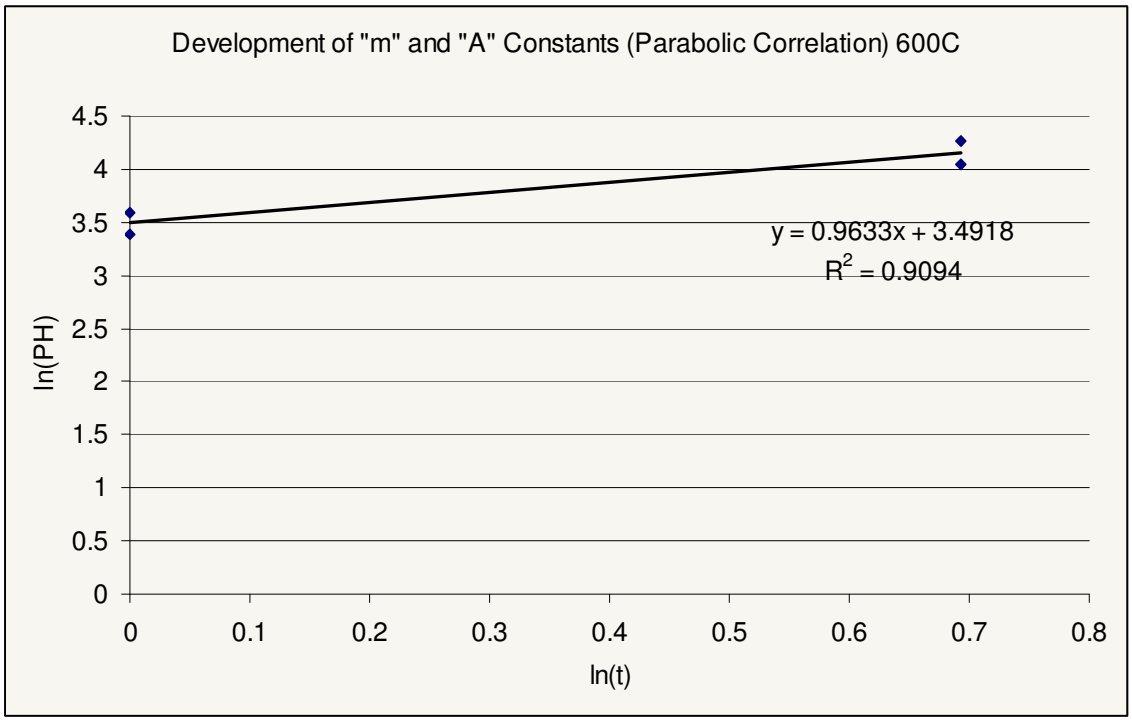
Development of "m" and "A" Constants (Parabolic Correlation) 600C
y = 0.9633x + 3.4918
R2 = 0.9094
ln(PH)
ln(t)
4.5
4
3.5
3
2.5
2
1.5
1
0.5
0
0
0.1
0.2
0.3
0.4
0.5
0.6
0.7
0.8

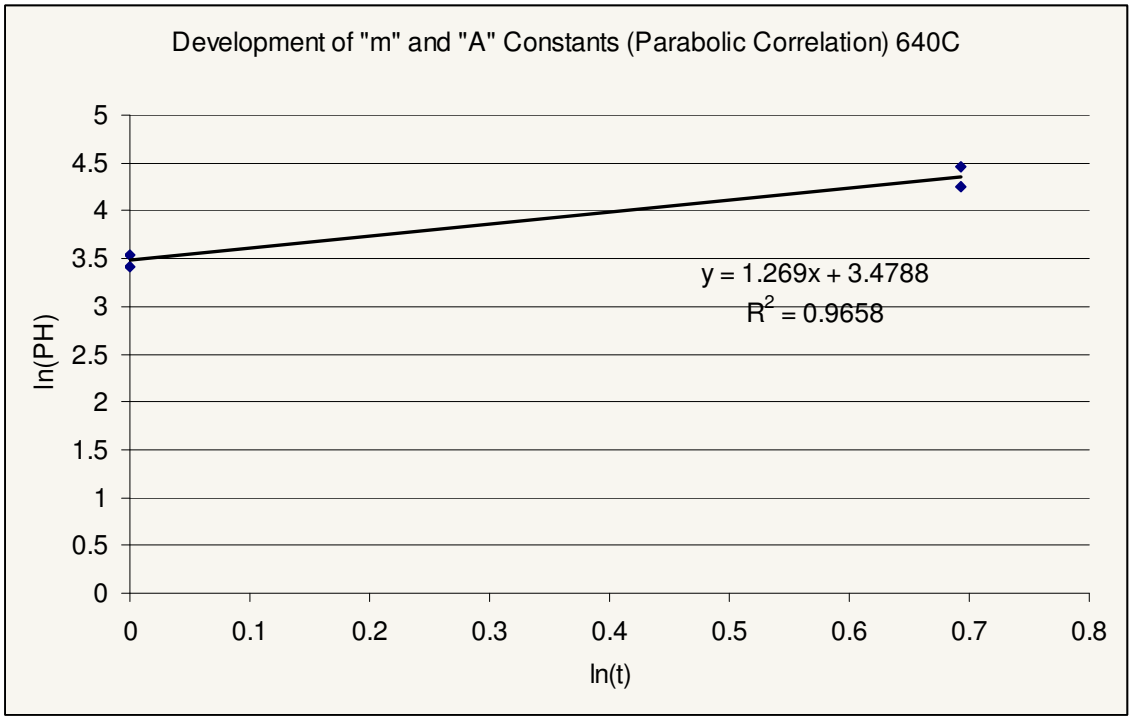
Development of "m" and "A" Constants (Parabolic Correlation) 640C
y = 1.269x + 3.4788
R2 = 0.9658
ln(PH)
ln(t)
5
4.5
4
3.5
3
2.5
2
1.5
1
0.5
0
0
0.1
0.2
0.3
0.4
0.5
0.6
0.7
0.8

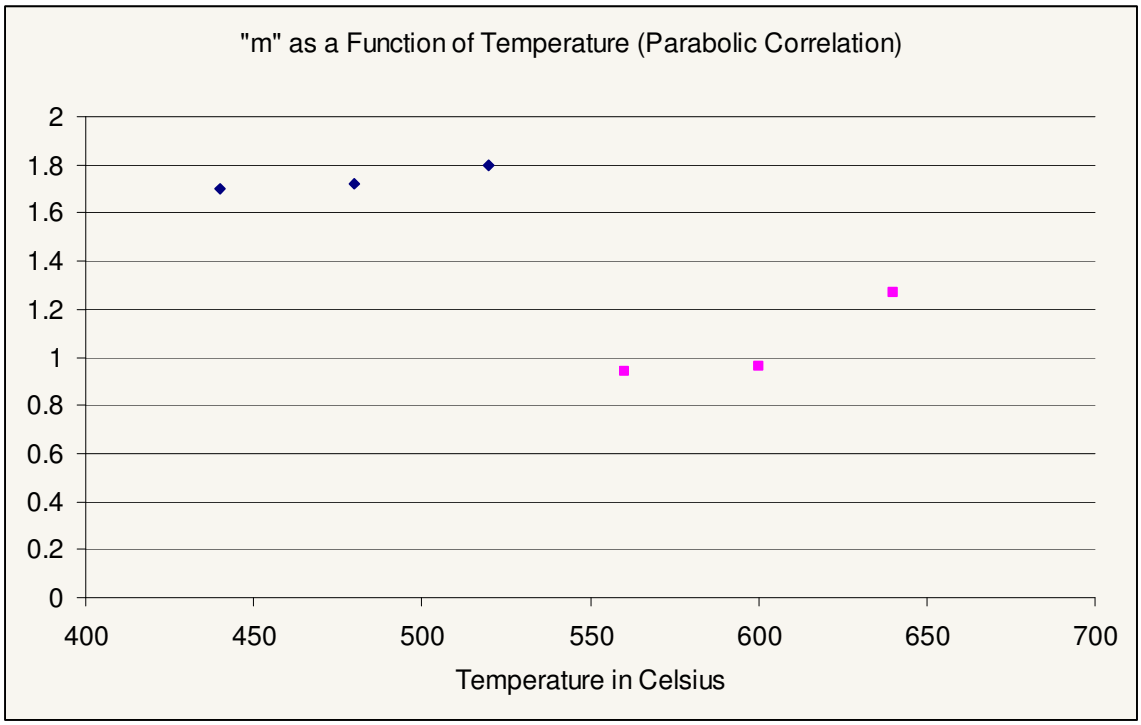
"m" as a Function of Temperature (Parabolic Correlation)
2
1.8
1.6
1.4
1.2
1
0.8
0.6
0.4
0.2
0
400
450
500
550
600
650
700
Temperature in Celsius

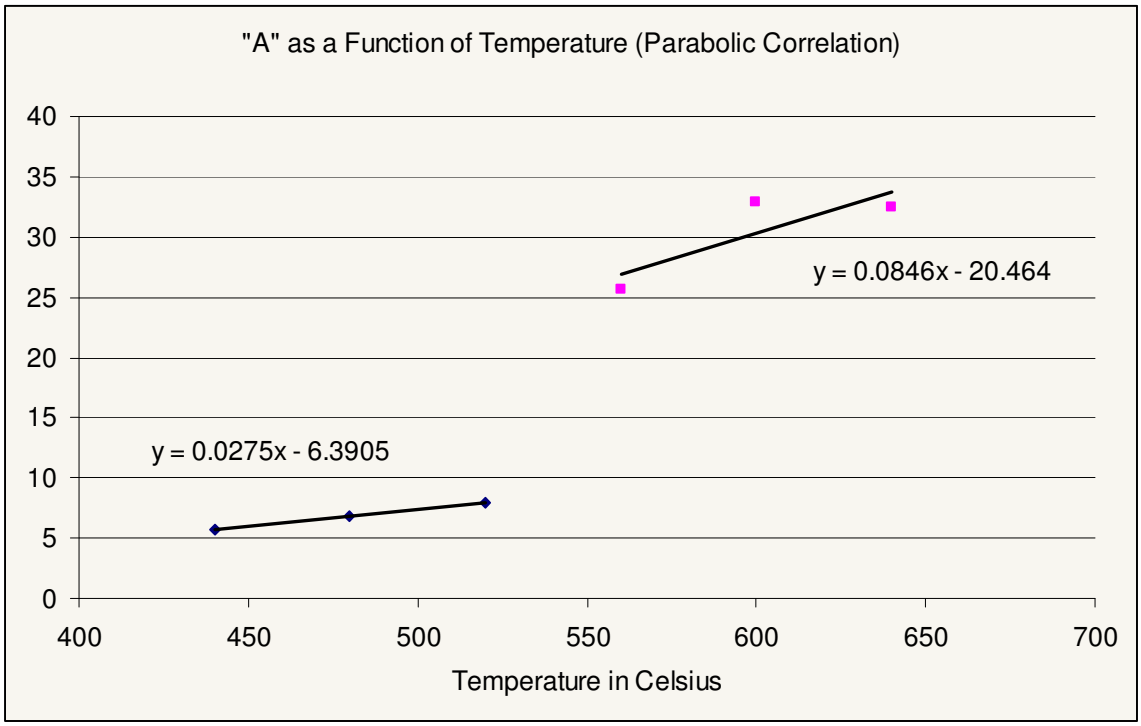
"A" as a Function of Temperature (Parabolic Correlation)
40
35
30
25
20
15
10
5
0
y = 0.0846x - 20.464
y = 0.0275x - 6.3905
400
450
500
550
600
650
700
Temperature in Celsius

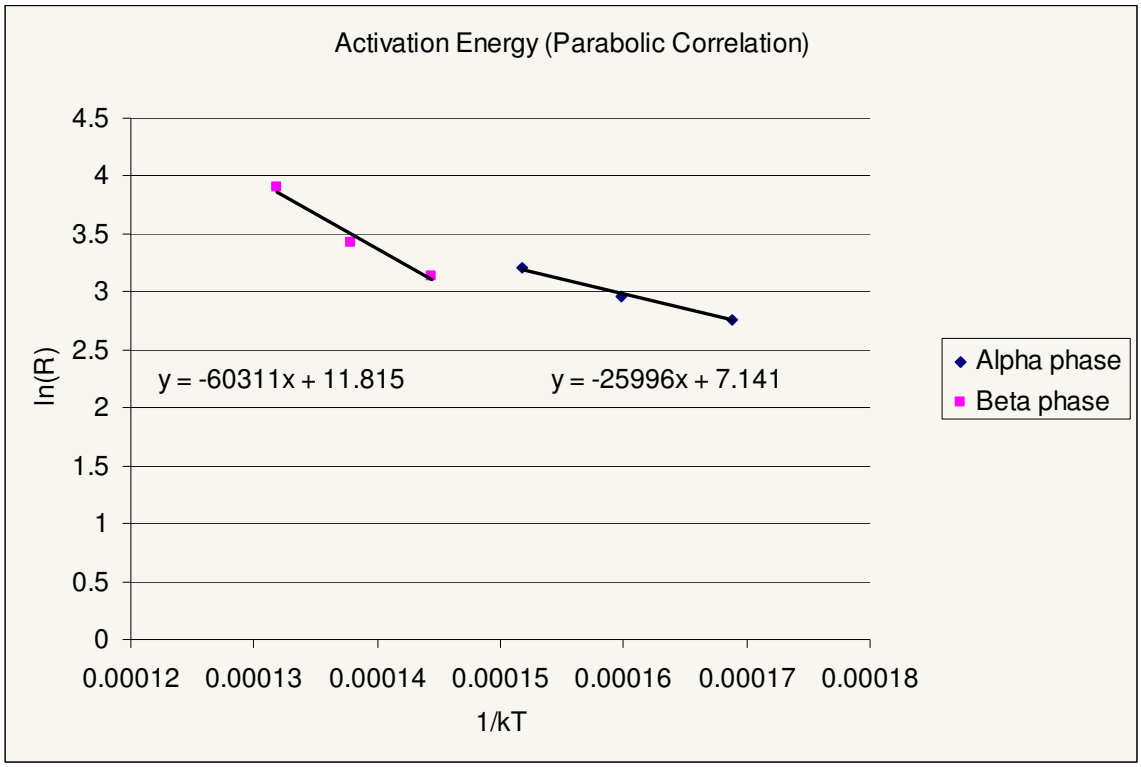
Activation Energy (Parabolic Correlation)
4.5
4
3.5
3
2.5
2
1.5
1
0.5
0
ln(R)
y = -60311x + 11.815
y = -25996x + 7.141
0.00012
0.00013
0.00014
0.00015
0.00016
0.00017
0.00018
1/kT
Alpha phase
Beta phase

APPENDIX D

CONSTANTS AND Q VALUE FROM LINEAR CORRELATION

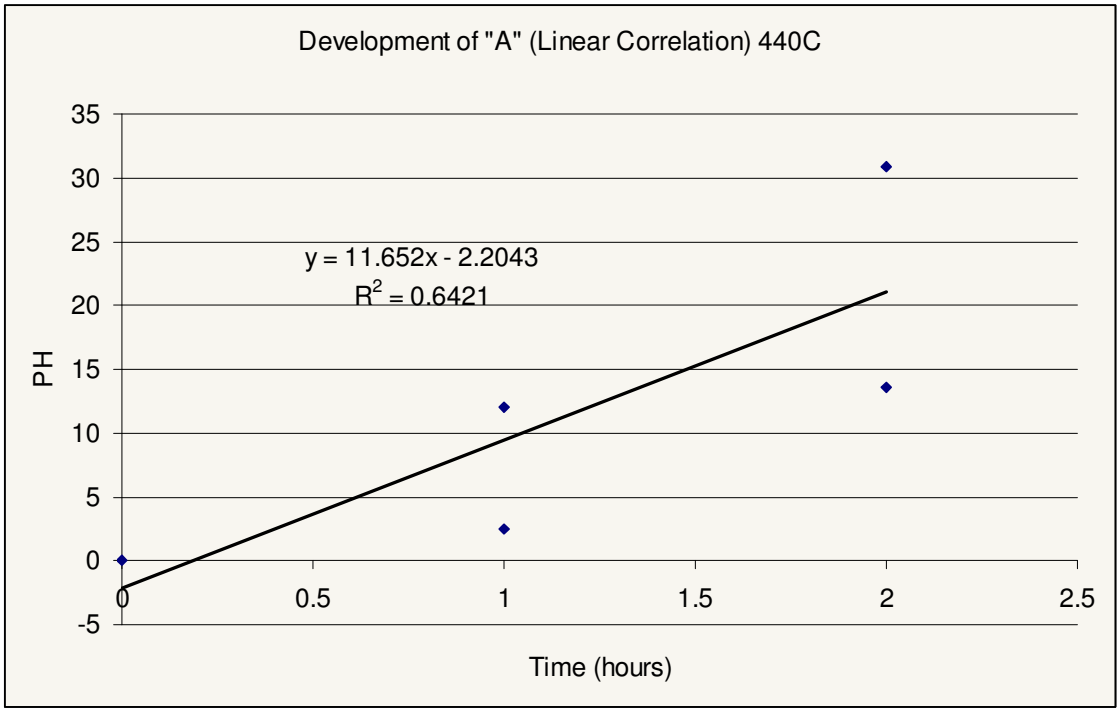

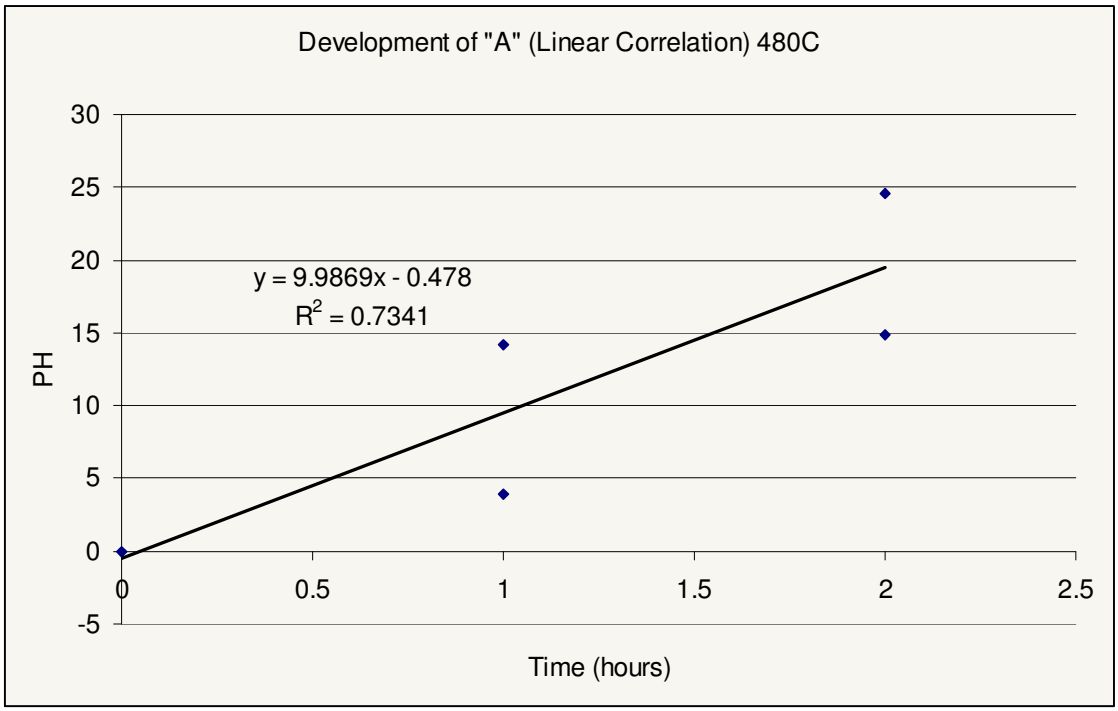

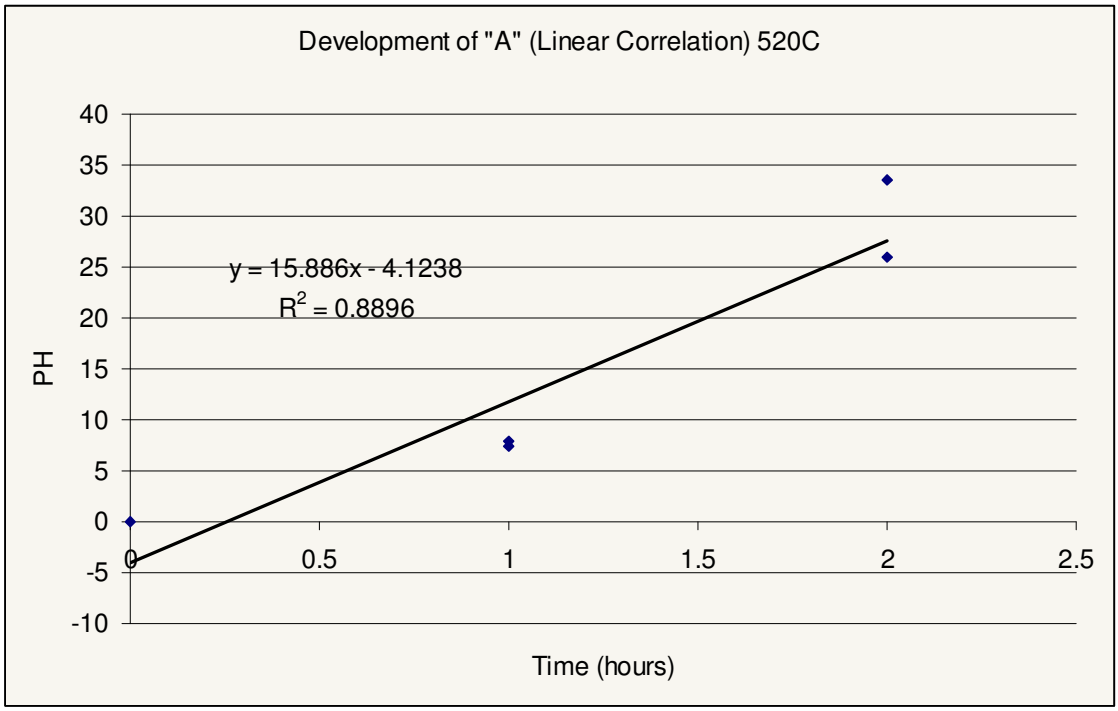
Development of "A" (Linear Correlation) 520C
y = 15.886x - 4.1238
R2 = 0.8896
PH
Time (hours)
40
35
30
25
20
15
10
5
0
-5
-10
0
0.5
1
1.5
2
2.5

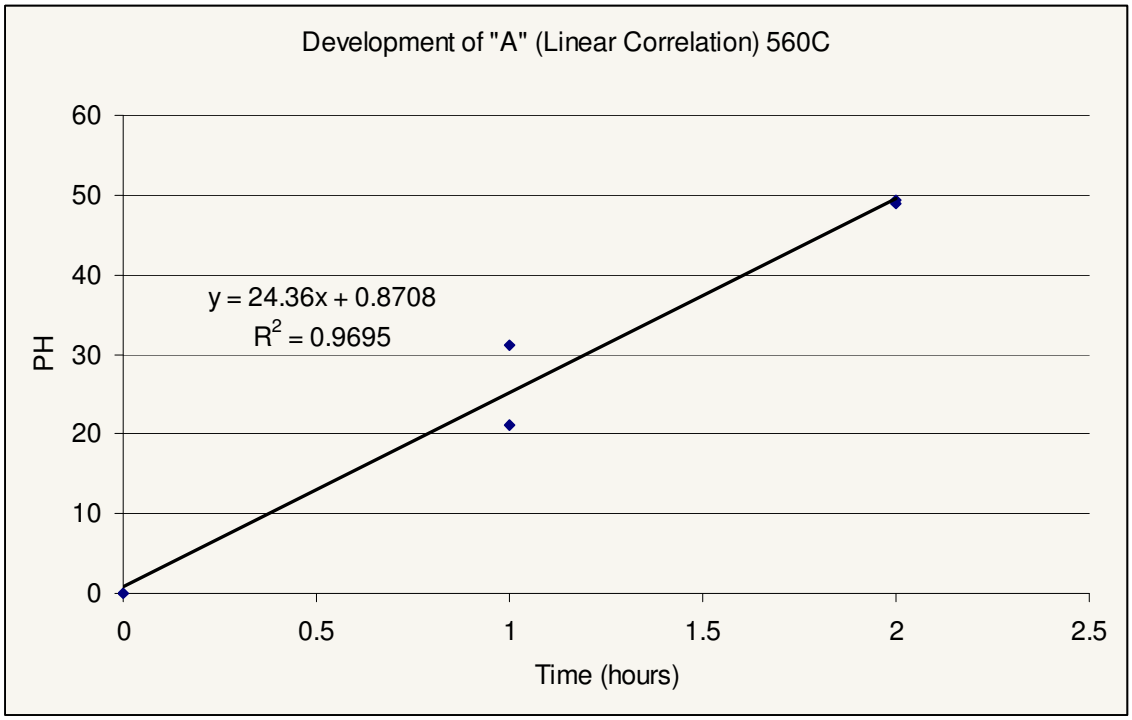
Development of "A" (Linear Correlation) 560C
y = 24.36x + 0.8708
R2 = 0.9695
PH
Time (hours)
60
50
40
30
20
10
0
0
0.5
1
1.5
2
2.5

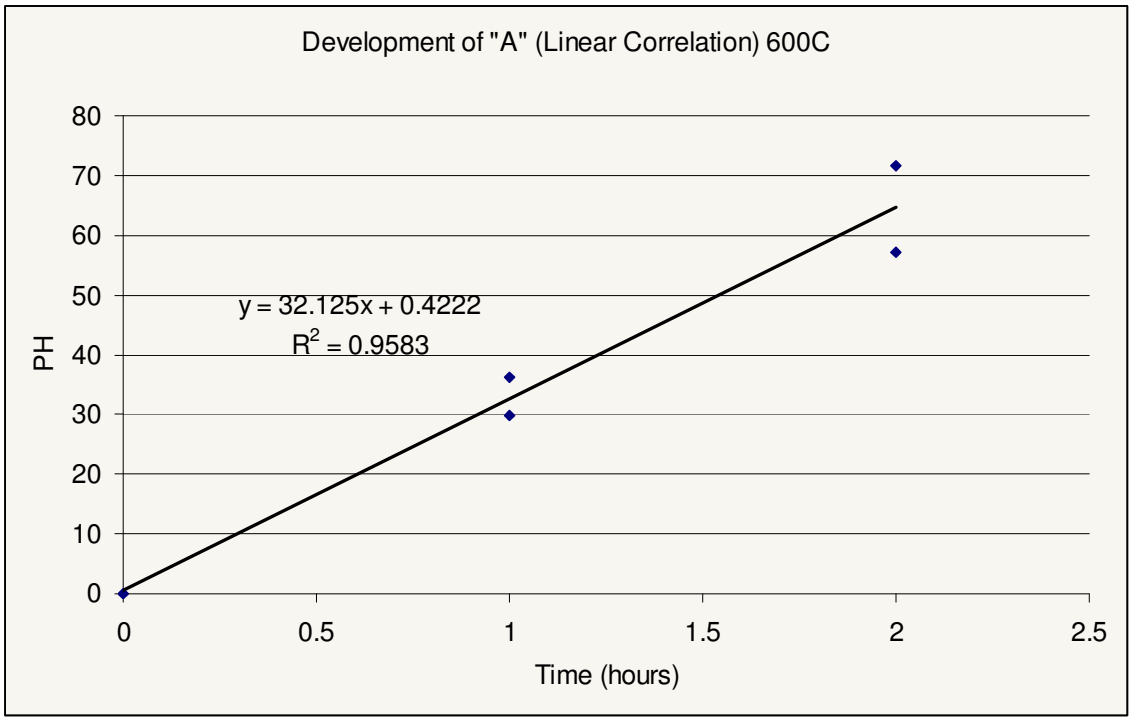
Development of "A" (Linear Correlation) 600C
y = 32.125x + 0.4222
R2 = 0.9583
PH
Time (hours)
0
10
20
30
40
50
60
70
80
0
0.5
1
1.5
2
2.5

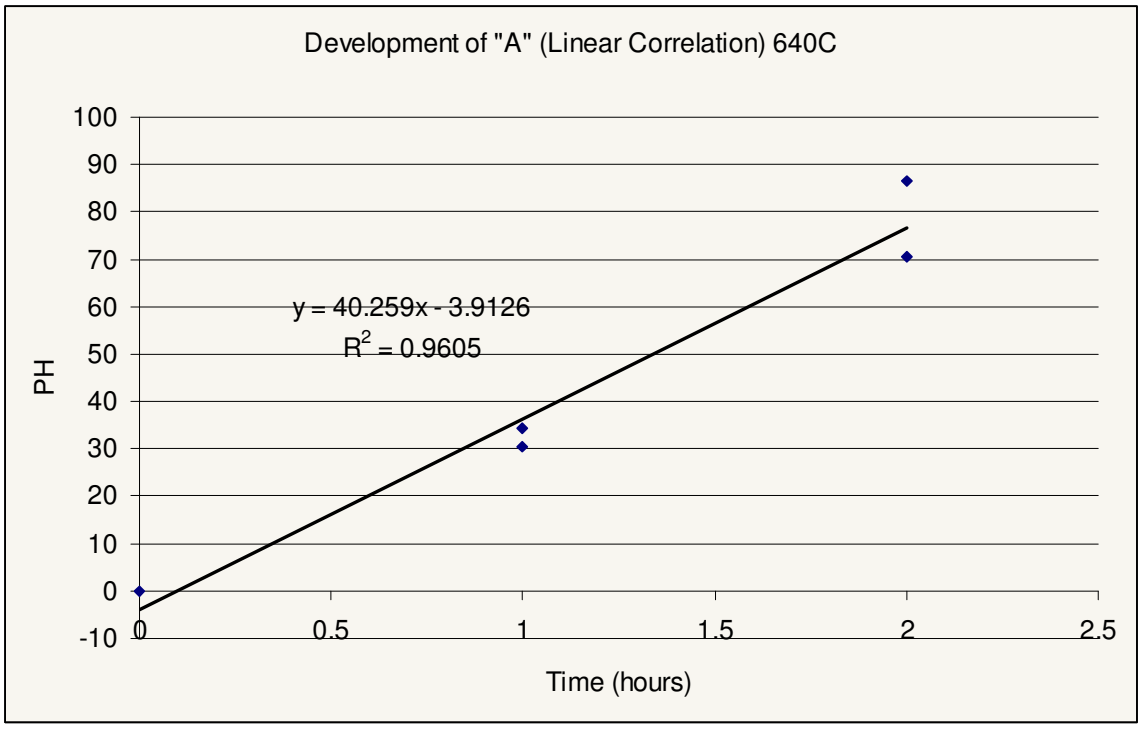
Development of "A" (Linear Correlation) 640C
y = 40.259x - 3.9126
R2 = 0.9605
PH
Time (hours)
-10
0
10
20
30
40
50
60
70
80
90
100
0
0.5
1
1.5
2
2.5

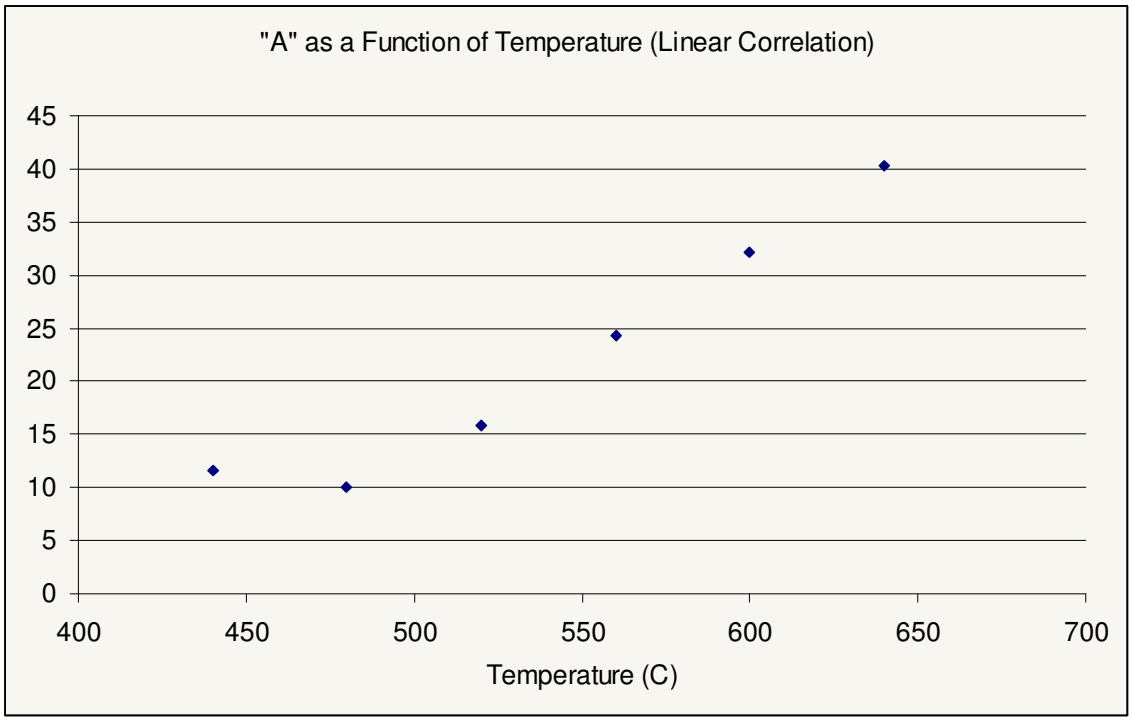
"A" as a Function of Temperature (Linear Correlation)
45
40
35
30
25
20
15
10
5
0
400
450
500
550
600
650
700
Temperature (C)

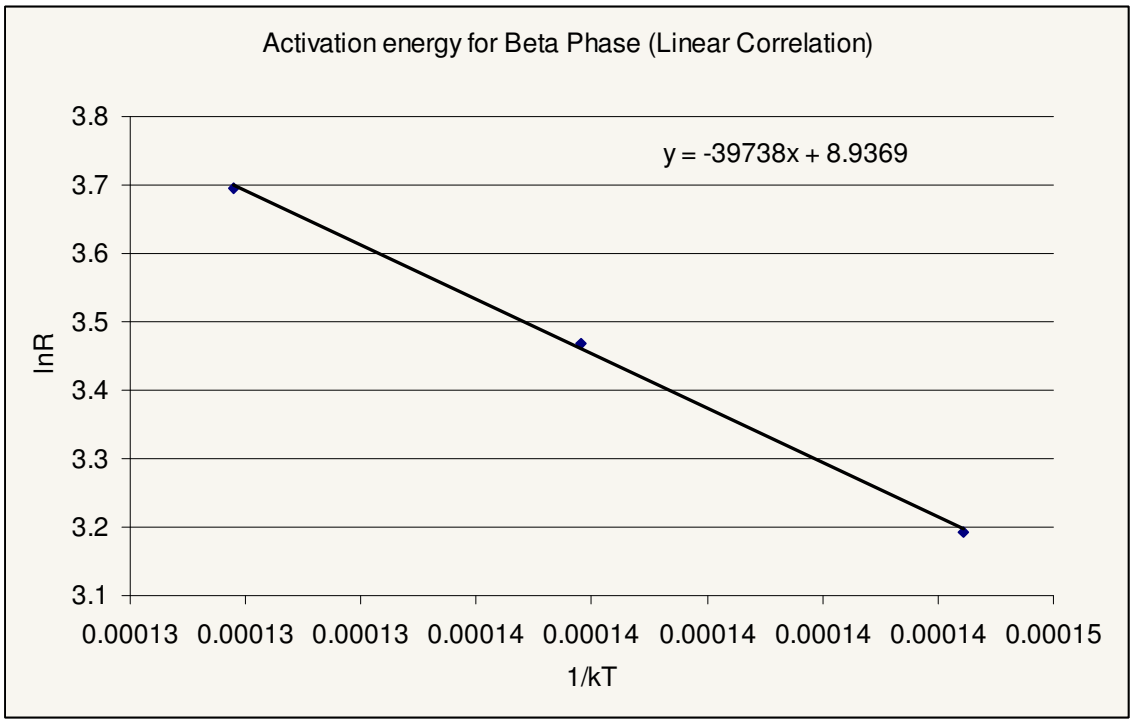
Activation energy for Beta Phase (Linear Correlation)
y = -39738x + 8.9369
3.8
3.7
3.6
3.5
3.4
3.3
3.2
3.1
lnR
0.00013
0.00013
0.00013
0.00014
0.00014
0.00014
0.00014
0.00014
0.00015
1/kT

VITA

Adam Joseph Parkison received his Bachelor of Science degree in nuclear engineering from Purdue University in 2006. He came to Texas A&M University in the fall of 2006 and graduated with a Master of Science degree in May 2008. His research interests include nuclear materials with an emphasis on new nuclear fuel forms, as well as the recycling of spent nuclear fuel.

Adam Parkison may be reached at Department of Nuclear Engineering, Texas A&M University, 3133 TAMU College Station, TX 77843-3133. His email address is ajparkison@tamu.edu.